CHAPTER-4

ENERGY ANALYSIS OF DOUBLE EFFECT H_2O–LiCl ABSORPTION REFRIGERATION SYSTEMS AND COMPARISON WITH H_2O–LiBr SYSTEMS

CHAPTER-4

ENERGY ANALYSIS OF DOUBLE EFFECT H_2O–LiCl ABSORPTION REFRIGERATION SYSTEMS AND COMPARISON WITH H_2O–LiBr SYSTEMS

4.1 Introduction

Vapour absorption refrigeration system (VARS) has received significant research interest in recent times. This was evident from the large number of research articles those were reviewed in Chapter 2. The major advantage is that low grade heat can be utilized for driving VARS. It was also mentioned in Chapter 1 that among the VARS configurations, the single effect system is the most commonly used. However, multi effect (double and triple effect) systems are also being considered for commercial use in refrigeration and HVAC industry due to higher COP of these systems. The triple effect system, although it provides the highest COP, but due to presence of more number of generators and other associated system components, additional cost and complexity are involved with the triple effect system. Hence among the multi effect systems, the double effect systems are gaining more popularity and finding more commercial use in the HVAC industry.

From the literature review in Chapter 2, it was found that performance of ASHRAE recommended double effect H_2O–LiCl VARS configurations have not been investigated in detail. There is not enough research articles related to H_2O–LiCl operated double effect VARS performance analysis except the articles [1, 2], where it was done separately for the series and parallel flow configurations. As such, the double effect series, parallel and reverse parallel VARS configurations were never compared earlier with H_2O–LiCl solution pair and thus, detail analysis is not available. Certainly, the effect of operating parameters on maximum allowable LiCl mass concentration limit (to avoid crystallization) and also on performance of double effect H_2O–LiCl absorption refrigeration systems would be different. This requires a detail investigation and therefore in this research study, the series, parallel and reverse parallel flow configurations of double effect H_2O–LiCl absorption refrigeration systems have been considered to analyze and compare their performance. A new set of thermodynamic property relations [3], which are valid for maximum up to 50% wt. concentration of H_2O–LiCl solutions, is considered in this Chapter. A parametric analysis is carried out to

show performance variation of the series, parallel and reverse parallel flow configurations of double effect H_2O–LiCl VARS with LPG and HPG temperatures against fixed evaporator, condenser and absorber temperatures. The effect of distribution ratio (*D*), on performance the double effect parallel and reverse parallel flow systems is also investigated. Further, the performances of the double effect H_2O–LiCl systems are compared with their counterparts operated with H_2O–LiBr pair under identical operating conditions. Details regarding performance of double H_2O–LiCl VARS configurations and their operational difference with corresponding double effect H_2O–LiBr VARS configurations are also highlighted in this chapter.

4.2 Description of the double effect absorption refrigeration systems

The schematics, the P–T–X and the enthalpy concentration diagrams of the three different double effect VARS configurations (series parallel and reverse parallel) are shown in Figs. 4.1–4.3. The presented double effect VARS configurations are similar to those which were earlier presented by Farshi et al. [4]. In the series configuration (Fig. 4.1a), the strong solution from the absorber is pumped directly to the HPG via the two solution heat exchangers (SHE I and SHE II). In the HPG, due to heat supply from steam, water vapour is generated and the medium concentration solution is produced which then goes to the LPG. In the LPG, the HPG off primary vapour provides the latent heat of condensation required for secondary vapour generation from the medium concentration solution and no external heat source is used. The medium solution after vapour generation in the LPG becomes weak which is then routed to the absorber via SHE I and expansion valve (ExV3). The LPG off condensed water and the secondary water vapour, both enters the condenser and the condensed liquid refrigerant (water) then goes to the evaporator through expansion valve 1 (ExV1). In the evaporator, the liquid refrigerant is evaporated which then goes to the absorber and dissolved with the weak refrigerant solution.

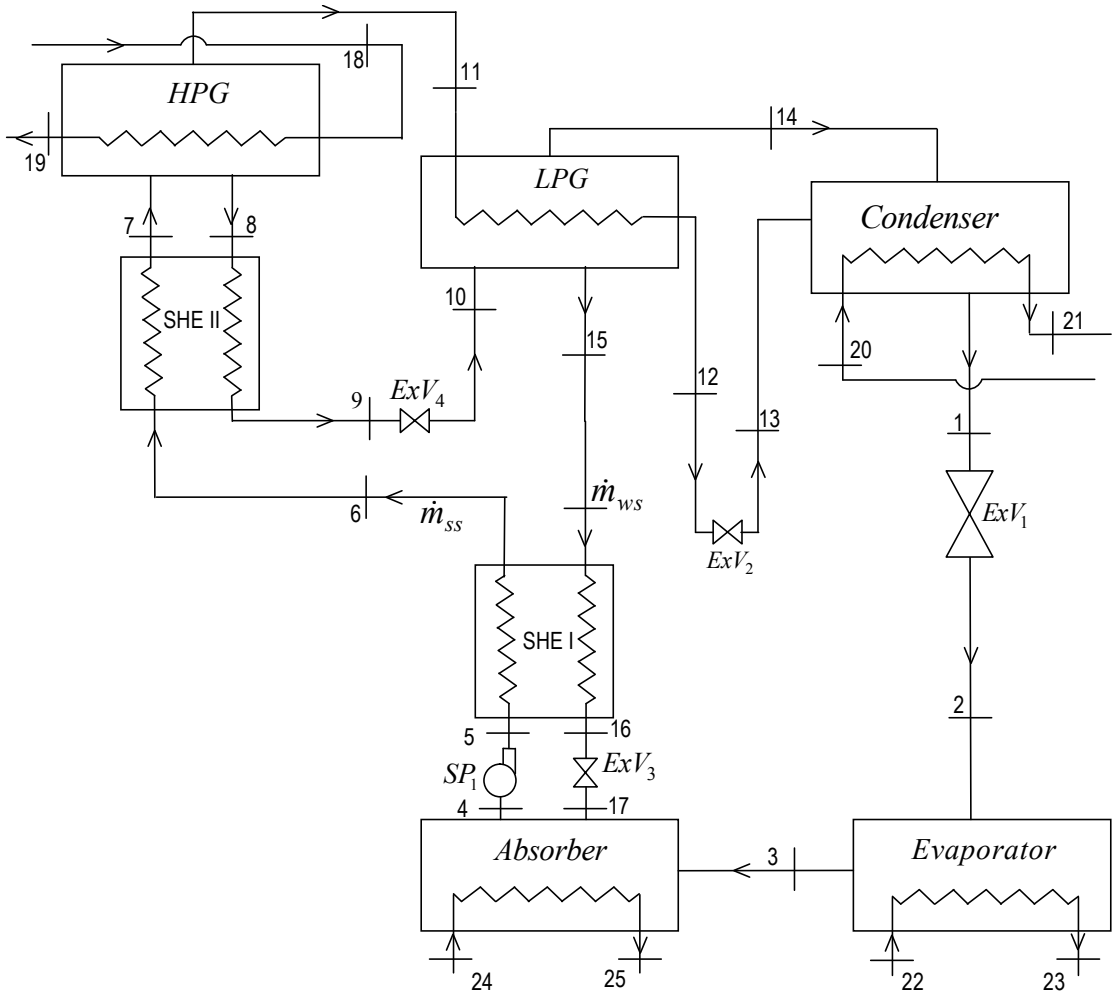

Fig. 4.1a**:** Schematic of a double effect VARS (Series configuration)

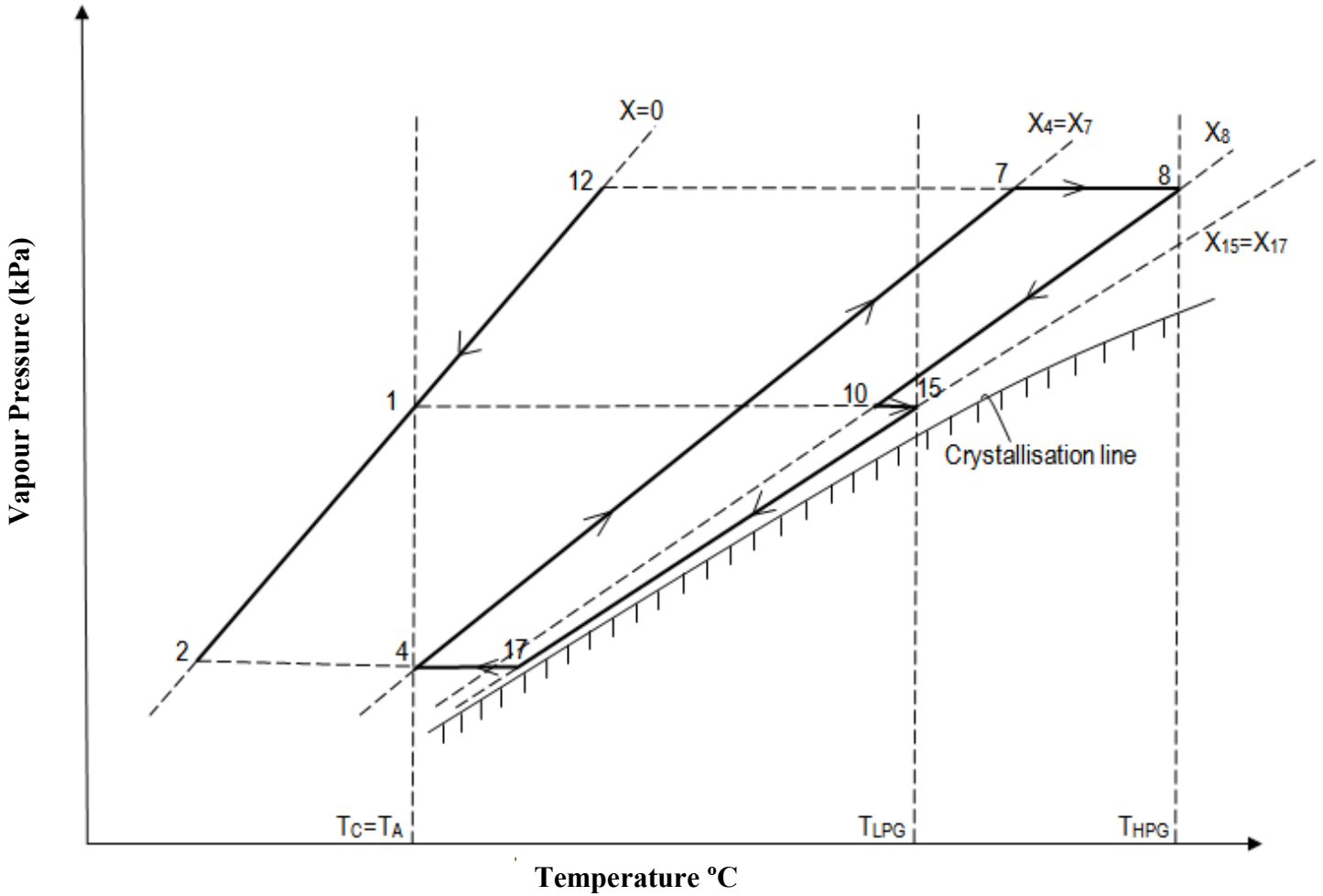

Fig. 4.1b**:** P−T−X diagram of double effect VARS (Series configuration)

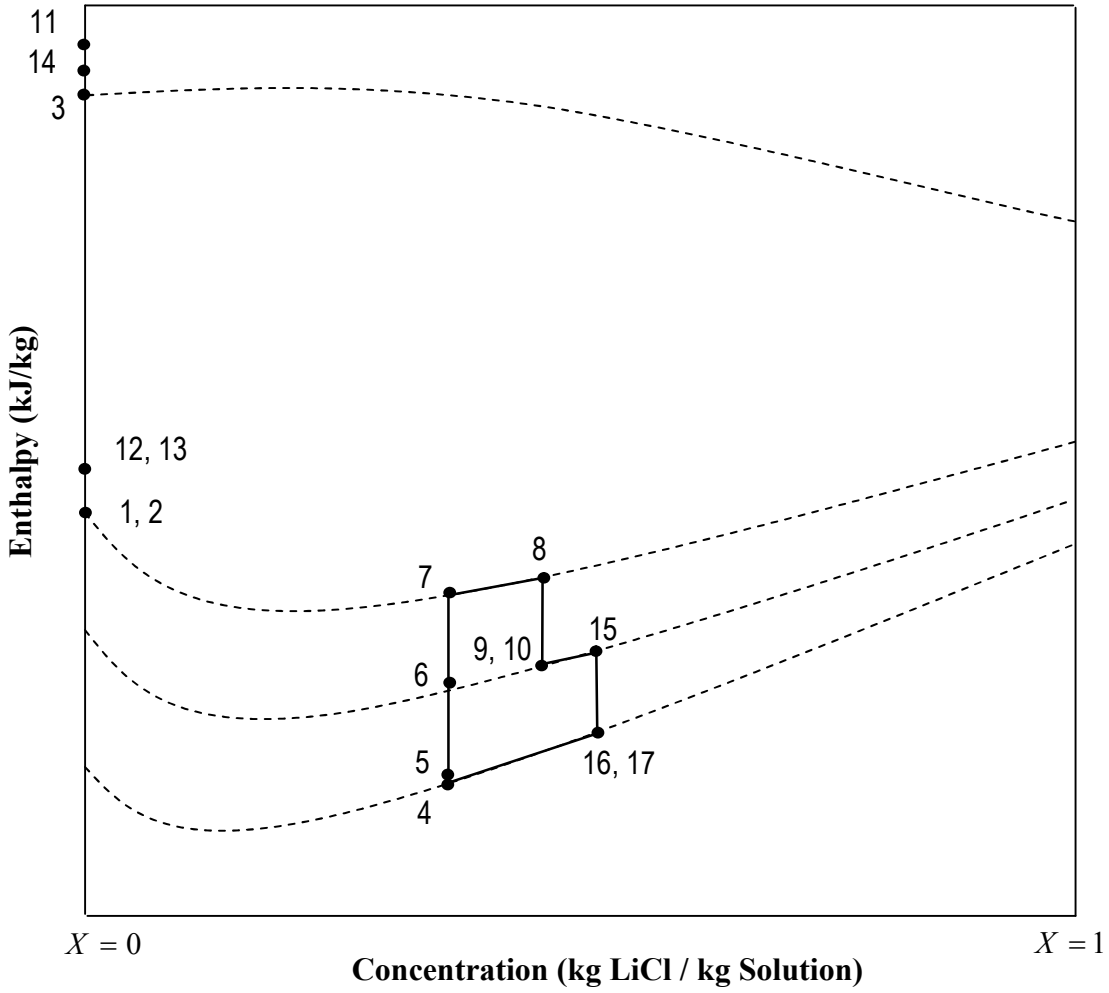

Fig.4.1c: Enthalpy–Concentration diagram (Series configuration)

In the parallel configuration (Fig. 4.2a), the absorber leaving strong solution from the absorber is distributed among the LPG and the HPG. The strong refrigerant solution after passing through SHE I, is divided into two streams: one stream goes to the LPG via expansion valve 4 (ExV4) and the other stream enters the HPG via SHE II. The medium concentration solution from the HPG flows back via SHE II and expansion valve 5 (ExV5) which then mix with the LPG off weak solution before it finally enters the absorber via SHE I and ExV3.

In the reverse parallel flow configuration (Fig. 4.3a), the absorber leaving strong solution first goes to the LPG via SHE I for partial vapour generation where the weak refrigerant solution is also produced. The LPG off weak solution is divided into two parts: one part is pumped to the HPG via SHE II and the other part is mixed with the HPG off medium concentration solution before it is routed to the absorber via SHE II

and ExV3. As such, two SPs are required in the reverse parallel configuration compared to one in the series and parallel configurations. Similarly in the series and reverse parallel configurations, total four expansion valves are required while in the parallel configuration, total five expansion valves are used.

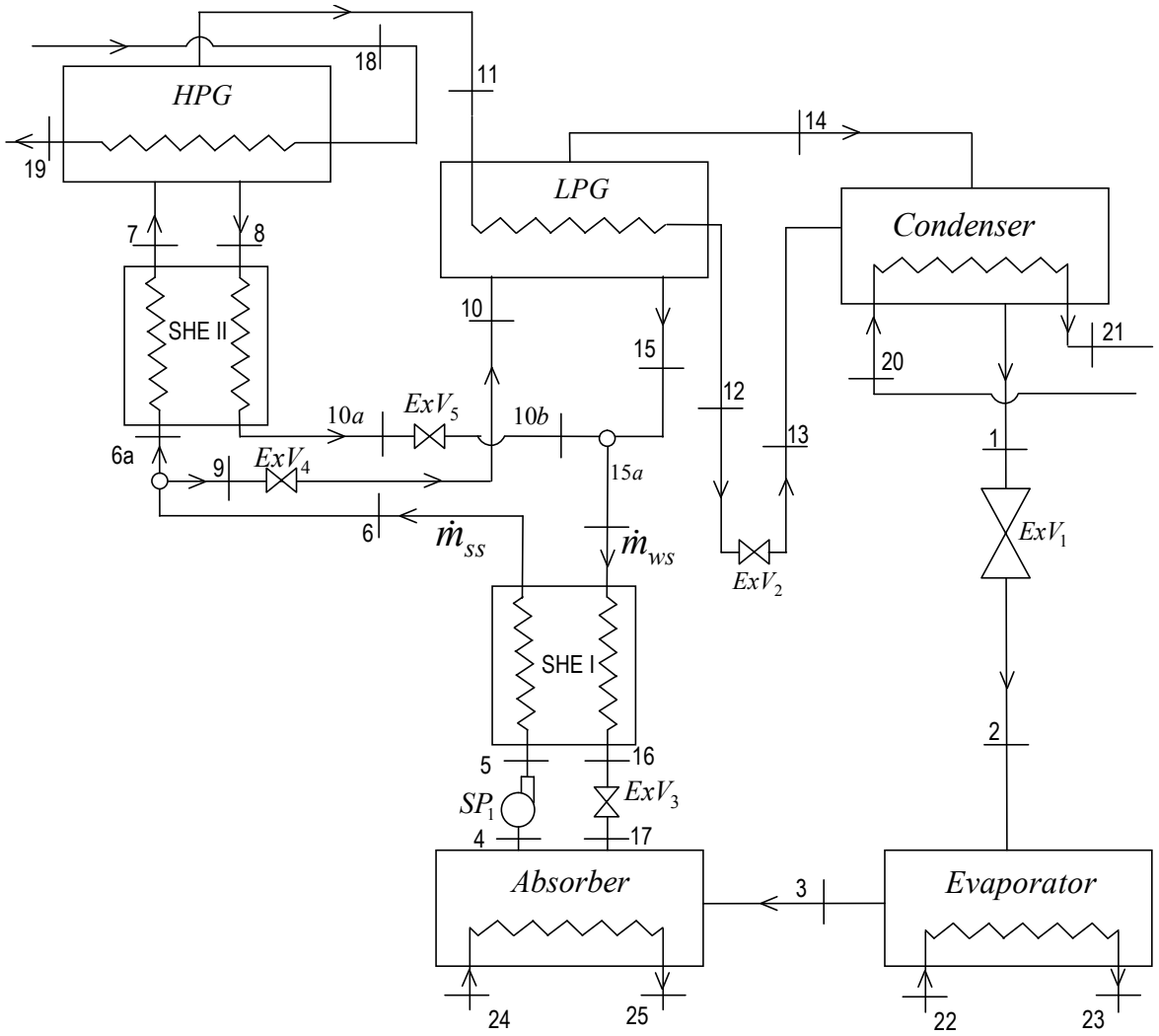

Fig. 4.2a**:** Schematic of a double effect VARS (parallel configuration)

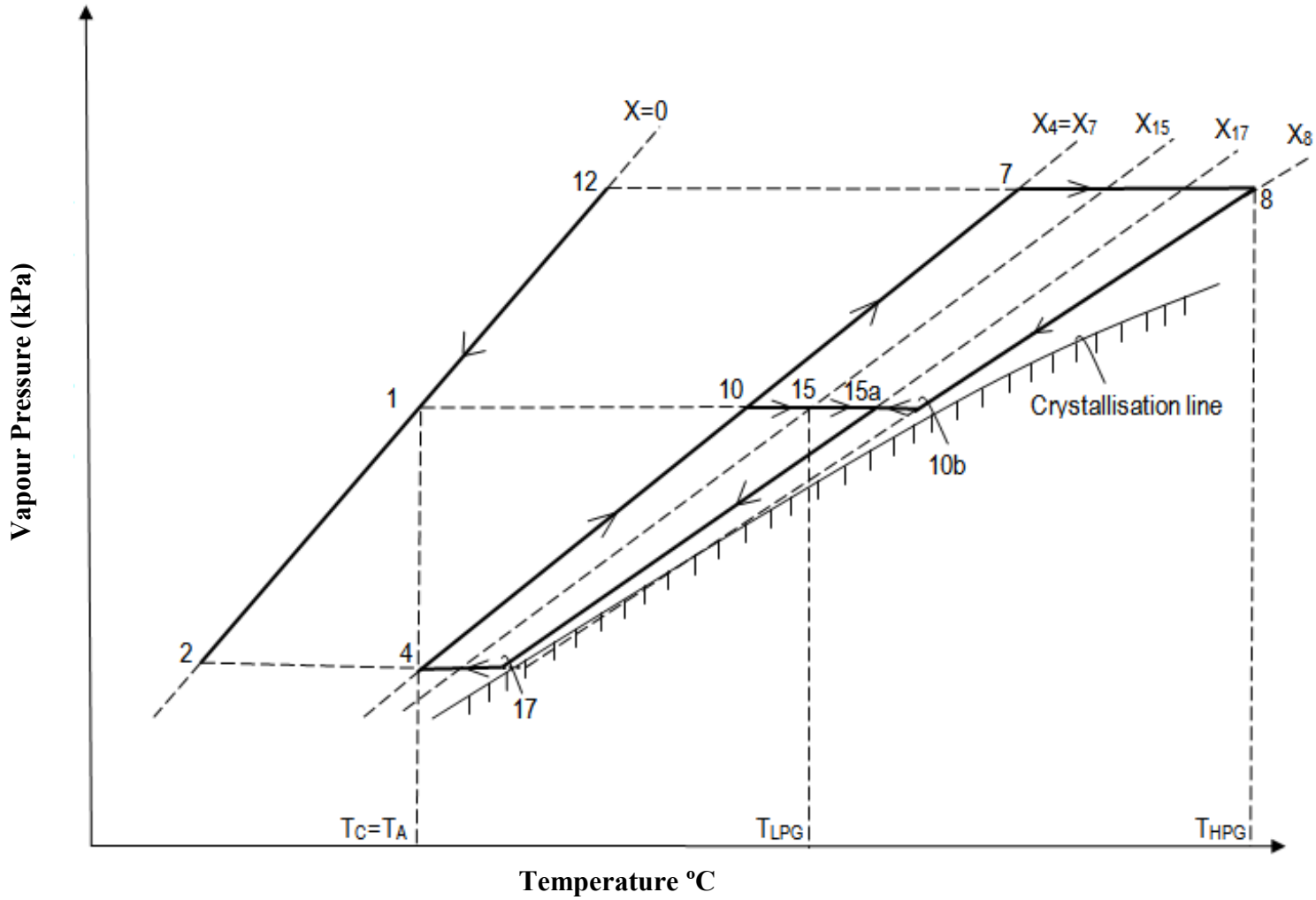

Fig. 4.2b**:** P−T−X diagram of double effect VARS (Parallel configuration)

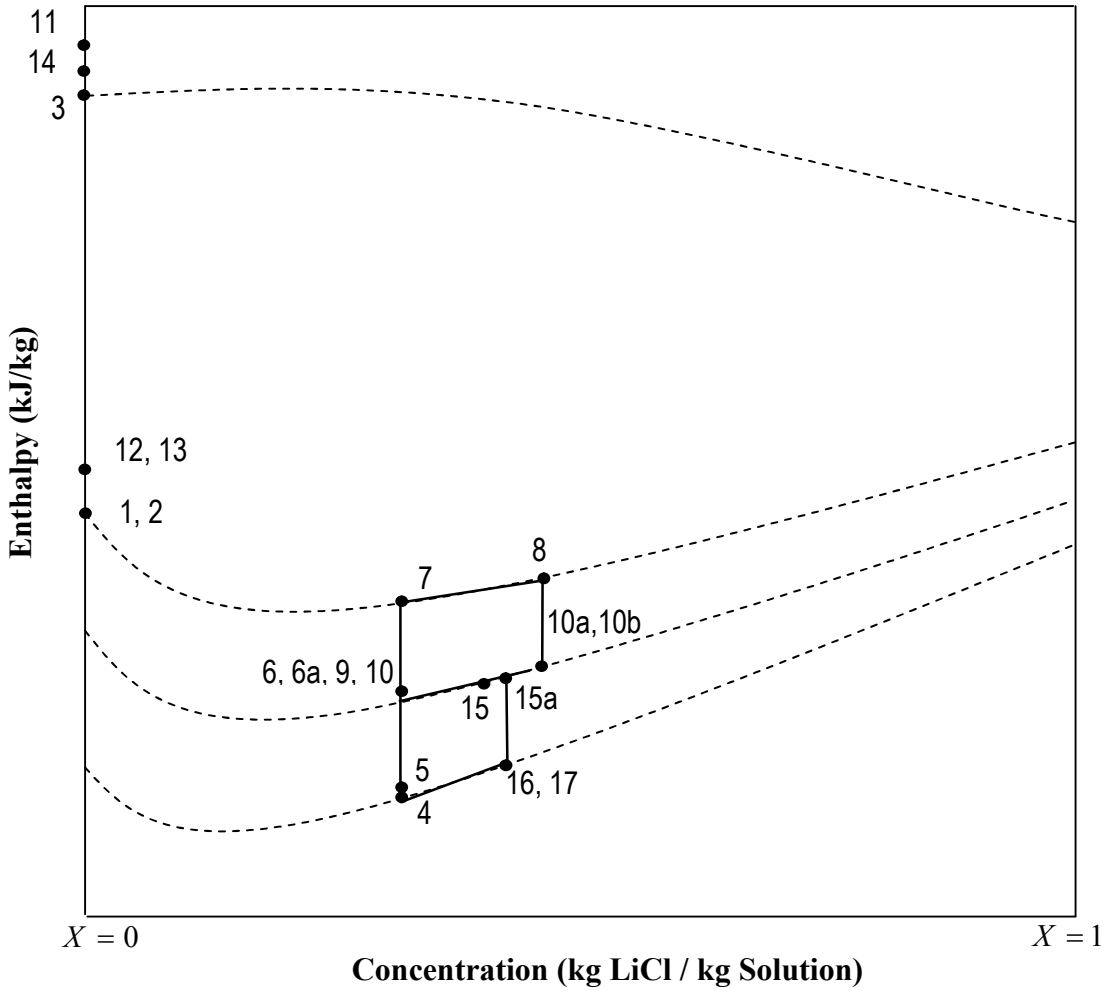

Fig.4.2c: Enthalpy–Concentration diagram (Parallel configuration)

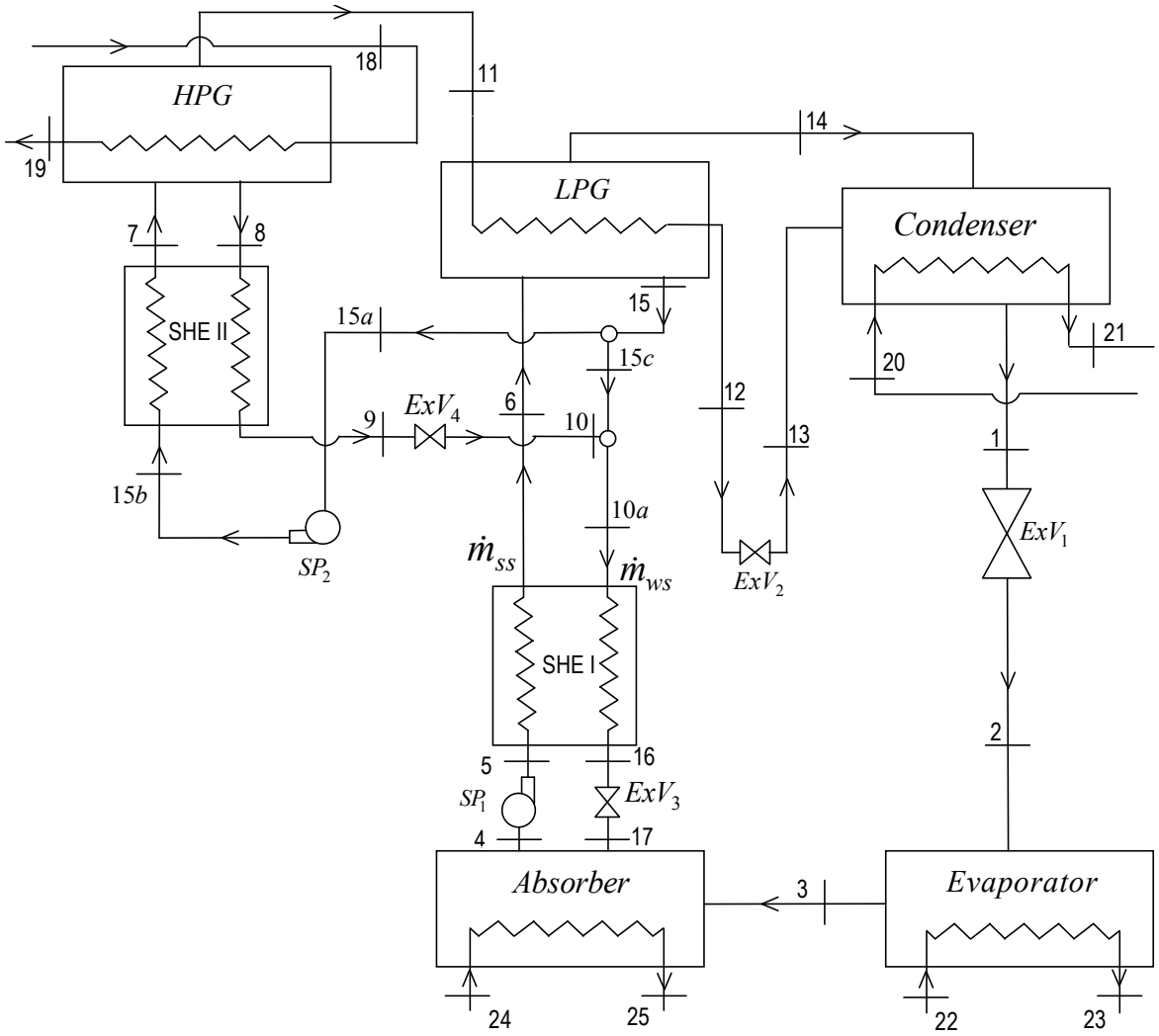

Fig. 4.3a**:** Schematic of a double effect VARS (reverse parallel configuration)

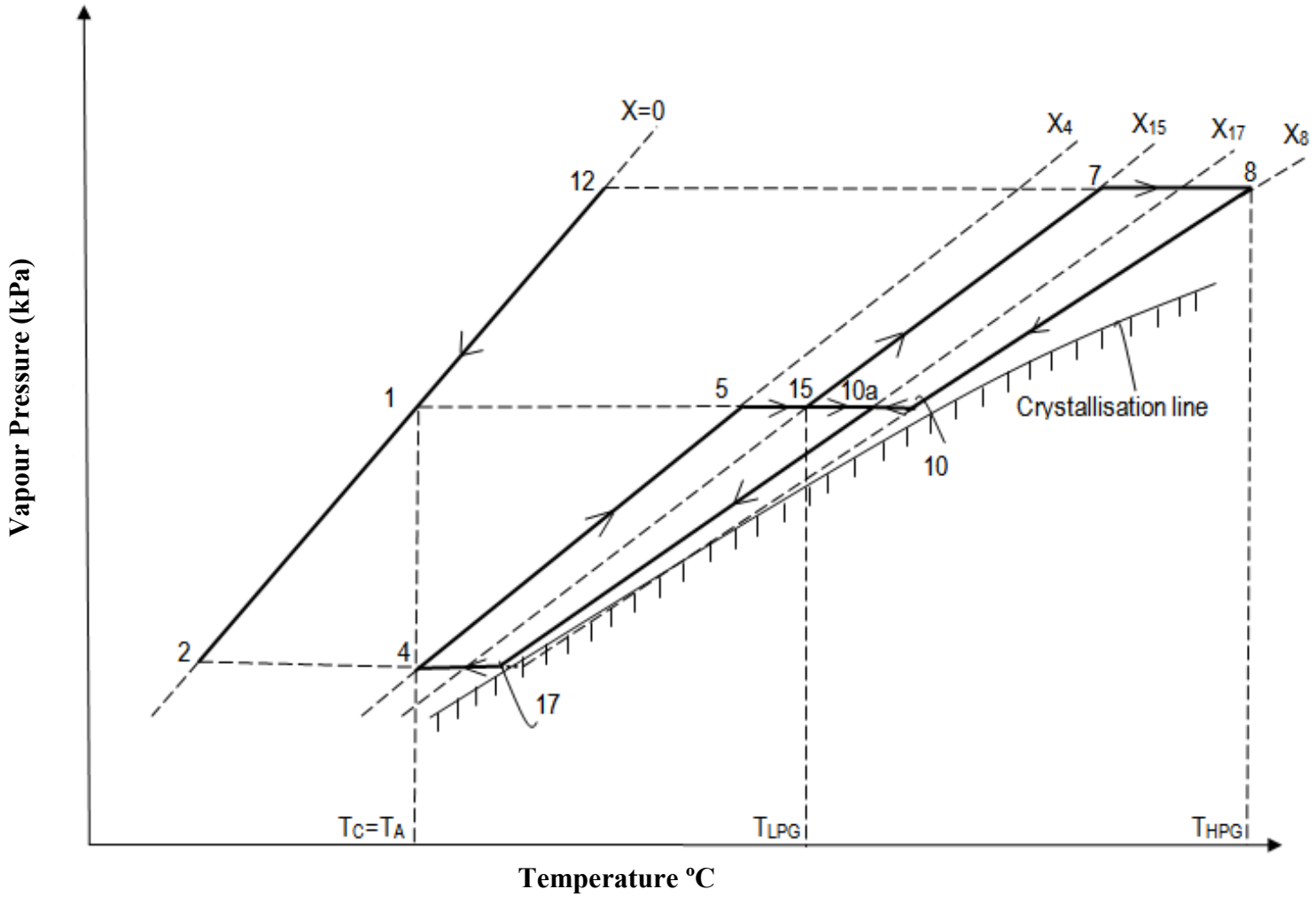

Fig. 4.3b**:** P−T−X diagram of double effect VARS (Reverse parallel configuration)

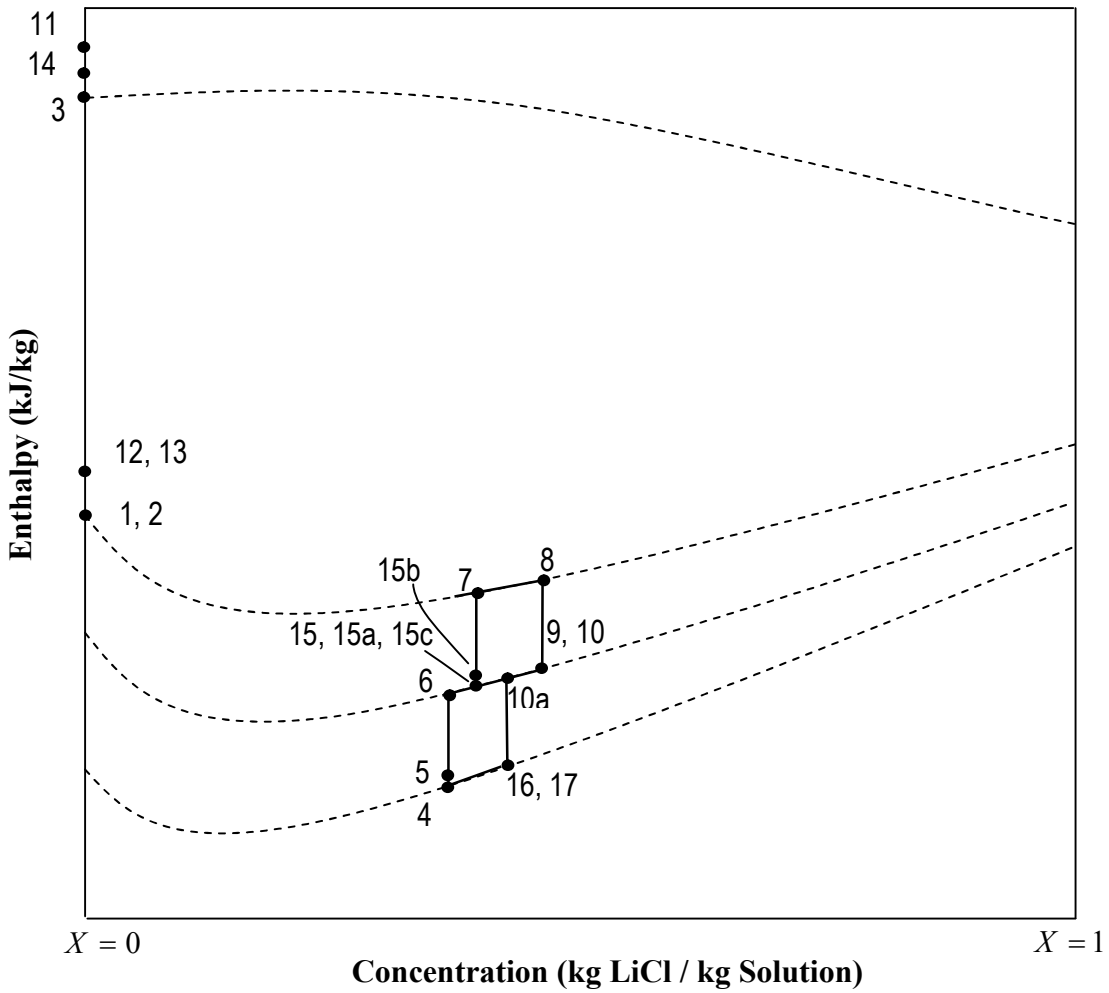

Fig.4.3c: Enthalpy–Concentration diagram (Reverse Parallel configuration)

4.3 Modeling assumptions

For energy analysis of the double effect systems also, certain assumptions are made in aligned with the assumptions of some previous studies [4, 5, 6, 7, 8, 9]. It is assumed that the systems operate under steady state. Heat loss between the system and surroundings is negligible. Pressure losses in the pipelines and heat exchangers are neglected. The refrigerant (water) is saturated liquid at condenser exit and saturated vapour at the evaporator outlet. Further, it is assumed that the absorber and evaporator pressures are equal. Similarly, condenser and LPG pressure are also assumed same. It is also assumed that the strong refrigerant solution at absorber exit is saturated liquid mixture at absorber temperature and pressure. Medium and weak solutions at HPG and LPG exits are saturated liquid mixtures at their respective generator temperature and pressure. HPG heat source is saturated steam with its saturation temperature 10°C higher than the HPG temperature. Simulation is carried out for a fixed cooling load of 350 kW. Motor efficiency is taken as 90% while the efficiencies of SHE I and SHE II are taken as 75%. Water temperatures at inlet and outlet of the condenser and absorber are considered as 25°C and 30°C respectively. For condensation of refrigerant vapour in the condenser, the vapour needs to reject heat to water and therefore, the water temperatures must be less than that of the condenser temperature (T_C). For this reason, the water temperature at condenser exit is considered 30°C to maintain a minimum 3°C of terminal temperature difference. In the absorber also, for the same reason, the water inlet and outlet temperatures are considered to be less than that of the absorber temperature (T_A) for effective heat transfer between the two mediums. In fact, similar water temperatures (25°C and 30°C) at inlet and outlet of the condenser and absorber were considered in the Ref. [5]. Evaporator inlet and outlet water temperatures are taken as 15°C and 10°C respectively. It can be assumed that the chilled water coming out from the evaporator at 10°C can cool and dehumidify certain amount of hot and humid moist air in air conditioning (AC) apparatus. After receiving heat from the AC apparatus, the temperature of water at AC apparatus exit will increase and therefore, the water temperature at evaporator inlet is assumed 15°C.

4.4 Mathematical Modeling of the double effect VARS configurations

Thermodynamic properties of H_2O–LiCl solution are calculated using the correlations of Patek and Klomfer [3]. The medium solution concentration at the HPG

exit (X_8) depends on pressure and temperature in the LPG, HPG, evaporator, absorber and the condenser. This is calculated in an iterative manner such that it satisfies the energy balance in the LPG [4]. For calculation of X_8, first the strong and weak solution concentrations (X_4 and X_{15}) at the outlets of the absorber and the LPG are required to be calculated. X_4 and X_{15} are also calculated iteratively using some specific set of equations (chemical potential) given in Ref. [3] from known pressure and temperature in these components. Details are shown in the Appendix. From known medium solution concentration at HPG exit (X_8) and HPG temperature (T_{HPG}), next the HGP pressure is determined using correlations given in Ref. [3] through iterative procedure. Thermodynamic properties of liquid water and water vapour (steam) are computed using equations taken from International Associations for the Properties of Water and Steam (IAPWS) formulation 1997 [10].

For all the three (series, parallel and reverse parallel flow) configurations, the following general mass and energy balance equations of steady flow processes are applied.

Mass conservation: $$\sum \dot{m}_{in} = \sum \dot{m}_{out} \tag{4.1}$$

$$\sum \dot{m}_{in} X_{in} = \sum \dot{m}_{out} X_{out} \tag{4.2}$$

Energy conservation: $$\sum \dot{Q} - \sum \dot{W} = \sum (\dot{m}h)_{in} - \sum (\dot{m}h)_{out} \tag{4.3}$$

The distribution ratio (D) is an important parameter for the double effect parallel (Fig. 4.1b) and reverse parallel flow (Fig. 4.1c) configurations which is defined as follows.

$$D_{parallel} = \frac{\dot{m}_{6a}}{\dot{m}_4} \tag{4.4}$$

$$D_{reverseparallel} = \frac{\dot{m}_{15a}}{\dot{m}_{15}} \tag{4.5}$$

From mass balance, the solution concentration at absorber inlet of the parallel and reverse parallel configurations, in terms of D, X_8 and X_{15}, can be expressed as follows.

$$X_{17} = \frac{1}{\left[\frac{D}{X_8} + \frac{1-D}{X_{15}}\right]} \tag{4.6}$$

Effectiveness method is used to calculate solution temperatures at the outlets of SHE I and SHE II. The mass flow rates of refrigerant $(\dot{m}_r)$ in the double effect series, parallel and reverse parallel systems are determined from known evaporator cooling load $(\dot{Q}_E)$ as follows.

` $$\dot{m}_r = \frac{\dot{Q}_E}{h_3 - h_2} \tag{4.7}$$

The amount of steam required in the HPG of the double effect series, parallel and reverse parallel systems are calculated using the following equations.

$$\dot{m}_{s,G} = \frac{\dot{Q}_{HPG}}{h_{18} - h_{19}} \tag{4.8}$$

where, $\dot{Q}_{HPG}$ is the heat load in the HPG.

COP of the double effect systems are determined as follows.

$$COP = \frac{\dot{Q}_E}{\dot{Q}_{HPG} + \dot{W}_{SP}}, \quad \dot{W}_{SP} \text{ is the SP pumping work.} \tag{4.9}$$

The modeling procedure adopted for simulation of double effect VARS configurations is same for both H_2O–LiCl and H_2O–LiBr solution pairs. Thermodynamic property relations for H_2O–LiBr are taken from Patek and Klomfar [9].

4.5 Validation

Not much experimental data related to VARS performance is available in the literature; neither for H_2O–LiBr nor for H_2O–LiCl operated double effect systems. Contrary to this, a good number of theoretical studies on H_2O–LiBr systems are available in the literature. In many theoretical studies related to VARS performance analysis with H_2O–LiBr solution pair, the property equations of Patek and Klomfer [8] are used [4, 5, 8−11]. From measured experimental data, Kaita [12] also developed equations for calculations of vapour pressure, specific heat, enthalpy and entropy of H_2O–LiBr

solution to facilitate modeling of multi-effect absorption chillers. Property equations of Kaita [12] are also used in VARS simulation [13]. For H_2O–LiCl solution also, experimental studies were carried out to develop equations for determining properties through curve fitting of experimental results [3, 14−16]. As such, the property model equations of Patek and Klomfar [3] are the most recent ones. Moreover, entropy related information of H_2O–LiCl solution is given only in the Ref. [3]**.** To show that the calculated property values are accurate, the present results are compared in Table 4.1 with those of Patek and Klomfar [3, 11] separately for H_2O–LiCl and H_2O–LiBr. This comparison now shows the correct implementation of the model equations into a corresponding computer code in the sense that the results of Patek and Klomfar [3, 11] could be produced exactly by using their model equations**.** Further, vapor pressure and enthalpy of H_2O–LiCl solution are compared with the experimental results of Conde [14] and Chaudhari and Patil [16]. The comparison is shown in Table 4.2 which shows some deviation in the present results obtained from the model equations of Patek and Klomfar [3] with those of Refs. [14, 16]. It may be mentioned that the formulation of thermodynamic property relations by Patek and Klomfar [3] is also based on curve fitting of experimental data where they used total 136 experimental works containing more than 2921 data points on various thermodynamic properties of the LiCl–H_2O solutions.

It was also tried to validate the system model, which however was not possible for the H_2O–LiCl operated double effect VARS configurations due to lack of available results. A double effect series configuration was earlier modeled by Won and Lee [1] using H_2O–LiCl as working pair, but the modeling procedure and equations used for calculating properties of H_2O–LiCl were entirely different from the present ones. Recently She et al. [17] and Bellos et al. [2] also made use of H_2O–LiCl in modeling respectively a two stage and a double effect parallel VARS configuration but these configurations presented in Refs. [2, 17] are not similar with the ones presented in this Chapter. Instead, the system model validation is presented for the H_2O–LiBr based double effect series configuration in which, the simulation results are compared with the results of Gomri and Hakimi [9] and Farshi et al. [6]. The comparison is shown in Table 4.3 and Table 4.4. A good agreement between the present and the previously published results was observed except little deviations in the enthalpy values at state points 6, 7, 9 and 10. Due to this little change in the enthalpy value at state point 7, the HPG heat load ($\dot{Q}_{HPG}$) also changed slightly in Table 4.3 and consequently, COP value was found

slightly higher in this study than those of Gomri [9] and Farshi et al. [4] at same operating conditions.

The calculated enthalpy and entropy values of H_2O–LiBr solution were compared additionally with the results of Kaita [12] and it was found that the results match very well. Say for example, at a temperature of 200°C and 50% wt. concentration, the enthalpy and entropy values obtained from equations of Patek and Klomfar [11] in this study were found to be 448.864 kJ/kg ad 1.219 kJ/kgK respectively against 444.9 kJ/kg and 1.217 kJ/kgK reported by Kaita [12].

Attempt was also made to validate the present H_2O–LiBr based simulation results with those of Farshi et al. [6] for the double effect parallel and reverse parallel configurations. However, due to lack of information regarding LPG temperature, considered during T_{HPG}variation in Ref. [6], this could not be done. In fact, Farshi et al. [6] also validated their simulation results comparing with those of Gomri and Hakimi [9] only.

Table 4.1: Comparison of property values obtained from the computer program with values given in Patek and Klomfar [3] and Patek and Klomfar [11]

Property values of H_2O–LiCl given in Patek and Klomfar [3]							Property values obtained from the computer program				
X	T (K)	P (Pa)	ρ (mol/m^3)	h (J/mol)	s (J/molK)	C_p (J/molK)	P (Pa)	ρ (mol/m^3)	h (J/mol)	s (J/molK)	C_p (J/molK)
0.05	275	609.80381	55,395.50	-62.662	1.63868	70.206	609.84371	55,395.57	-62.663	1.63868	70.206
0.05	400	216,992.40	52,535.60	8685.800	27.8383	71.104	216990.431	52,535.67	8685.843	27.83835	71.104
0.1	300	2369.4499	54,664.00	1515.800	7.08674	66.084	2369.4502	54,664.01	1515.865	7.08674	66.084
0.1	400	174,068.99	52,775.20	8124.500	26.0841	66.863	174,068.38	52,775.23	8124.506	26.08416	66.863
0.2	275	144.8949	54,054.80	840.620	-.00299	66.297	144.8972	54,054.82	840.621	-0.0030	66.298
0.3	350	5105.0296	51,488.60	8358.500	15.0865	60.254	5105.0298	51,488.64	8358.501	15.08656	60.254
0.3	400	40,415.04	50,301.20	11365.400	23.1153	60.140	40,415.05	50,301.23	11365.454	23.11538	60.140
Property values of H_2O–LiBr given in Patek and Klomfar [11]							Property values obtained from the computer program				
X	T (K)	P (Pa)	ρ (mol/m^3)	h (J/mol)	s (J/molK)	C_p (J/molK)	P (Pa)	ρ (mol/m^3)	h (J/mol)	s (J/molK)	C_p (J/molK)
0.05	300	3025.1805	54148.9	1603.9	7.79057	69.931	3025.1805	54148.95	1603.851	7.79047	69.931
0.05	450	835,097.47	48984.9	12,189.00	36.5288	74.047	835097.48	48984.95	12188.91	36.5287	74.047
0.1	300	2286.4858	52985.4	1445.1	7.66416	65.52	2286.4858	52985.42	1445.004	7.66407	65.52
0.1	450	647,702.12	48550.2	11,555.20	34.9553	70.305	647702.12	48550.22	11555.09	34.9552	70.305
0.3	350	2237.3986	47826.4	9072.1	15.3214	66.597	2237.3986	47826.42	9072.022	15.3213	66.597
0.4	450	43,075.149	45941.8	21,024.40	33.3788	70.294	43075.149	45941.89	21024.33	33.3788	70.294

Table 4.2: Comparison of vapour pressure and enthalpy values obtained from the computer program with experimental results [16] and results of Conde [14]

		Temperature (°C)					
X (%)	Vapour pressure (kPa)	30	40	50	60	70	80
19.27	Conde [14]	3	5.24	8.8	14.27	22.42	34.22
	Experimental [16]	3.01	5.25	8.83	14.32	22.5	34.37
	Present study	3.23	5.64	9.46	15.33	24.05	36.66
36.98	Conde [14]	1.06	1.93	3.37	5.67	9.23	14.56
	Experimental [16]	1.03	1.87	3.28	5.54	9.06	14.37
	Present study	1.35	2.43	4.19	6.99	11.28	17.66
44.19	Conde [14]	0.55	1.04	1.86	3.21	5.35	8.62
	Experimental [16]	0.57	1.07	1.92	3.32	5.56	9
	Present study	0.77	1.42	2.51	4.28	7.06	11.29
X (%)	Enthalpy (kJ/kg)	30	40	50	60	70	80
20	Conde [14]	82.43	114.86	147.35	179.88	212.47	245.1
	Experimental [16]	82.5	115	147.5	180.1	212.6	245.3
	Present study	84.95	117.36	149.74	182.13	214.56	247.03
35	Conde [14]	108.87	137.24	165.6	193.94	222.27	250.59
	Experimental [16]	108.5	136.8	165.2	193.5	221.9	250.2
	Present study	89.44	116.99	144.39	171.66	198.86	226.00
45	Conde [14]	–	–	230.21	255.34	280.44	305.5
	Experimental [16]	–	–	230.9	256	281	306.1
	Present study	134.03	159.01	183.77	208.34	232.78	257.10

Table 4.3: Comparison of present results (double effect H_2O–LiBr series configuration) with those of Gomri and Hakimi [9] and Farshi et al. [6]

State Point	T (K)			$\dot{m}$ (kg/s)			X (%)			h (kJ/kg)	
	Gomri	Farshi	Present study	Gomri	Farshi	Present study	Gomri	Farshi	Present study	Farshi	Present study
1	308	308	308.15	0.127	0.127	0.127	-	-	-	146.59	146.64
2	277	277	277.15	0.127	0.127	0.127	-	-	-	146.59	146.64
3	277	277	277.15	0.127	0.127	0.127	-	-	-	2507.87	2508.20
4	308	308	308.15	1.737	1.735	1.736	55.869	55.88	55.87	87.67	87.66
5	308	308	308.17	1.737	1.735	1.736	55.869	55.88	55.87	87.67	87.70
6	335.49	335.49	336.62	1.737	1.735	1.736	55.869	55.88	55.87	143.14	145.17
7	379.81	379.8	381.58	1.737	1.735	1.736	55.869	55.88	55.87	235.43	238.87
8	403	403	403.15	1.671	1.67	1.671	58.056	58.07	58.05	288.40	288.37
9	349.09	356.09	356.58	1.671	1.67	1.671	58.056	58.07	58.05	192.49	193.15
10	349.09	356.09	356.58	1.671	1.67	1.671	58.056	58.07	58.05	192.49	193.15
11	403	403	403.15	0.065	0.065	0.065	-	-	-	2740.53	2741.00
12	355.46	355.45	355.62	0.065	0.065	0.065	-	-	-	345.21	345.34
13	308	308	308.15	0.065	0.065	0.065	-	-	-	345.21	345.34
14	353	353	353.15	0.062	0.062	0.062	-	-	-	2649.57	2650.00
15	353	353	353.15	1.61	1.608	1.609	60.278	60.294	60.280	195.84	195.82
16	321.67	321.67	321.66	1.61	1.608	1.609	60.278	60.294	60.280	135.98	135.67
17	321.67	321.67	321.66	1.61	1.608	1.609	60.278	60.294	60.280	135.98	135.67

Table 4.4: Comparison of component heat loads, SP power and COP of present study with those of Gomri and Hakimi [9] and Farshi et al. [4] at $T_C = T_A = 35$ºC, $T_E = 4$ºC, $T_{HPG} = 130$ºC, $T_{LPG} = 80$ºC, 70% SHE I and SHE II efficiencies and 95 % SP efficiency for the double effect series configuration

Parameter	Gomri [9]	Farshi [4]	Present study
HPG, ($\dot{Q}_{HPG}$ kW)	252.407	252.394	245.353
Condenser, $\dot{Q}_C$ kW	167.205	167.190	168.461
Evaporator, ($\dot{Q}_E$ kW)	300.000	300.000	300.000
Absorber, ($\dot{Q}_A$ kW)	385.236	385.203	384.716
SP, ($\dot{W}_{SP}$ kW)	≈ 0.000	0.033	0.058
COP	1.189	1.188	1.222

4.6 Results and Discussion

In this section, the computer simulation based performance results are shown separately for each of the double effect series, parallel and reverse parallel configurations. For each system, performance variation is shown with respect to T_{LPG} and T_{HPG} for three cases of condenser and absorber temperatures (T_C and T_A) viz. 33°C, 35°C and 38°C respectively where T_C and T_A values are assumed equal. Performance variation is also shown for two evaporator temperatures viz. T_E =8°C and T_E =5°C. In case of the parallel and reverse parallel systems, the distribution ratio *(D)* is varied to show its effect on COP and also to find the optimum *D* with respect T_{LPG} and T_{HPG} variations. The ranges of T_{LPG} and T_{HPG} for the three systems and *D* in case of the parallel and reverse parallel systems are selected in such a way that in no case, the H_2O–LiCl solution concentration exceeds 50% limit. Simulation of the three systems is carried out for a constant evaporator cooling load of 350 kW. During T_{HPG} variation, the distribution ratio *D* for the parallel and reverse parallel systems are kept fixed at 0.5. This is at this *D*, actually the COPs of the parallel and reverse parallel systems are found maximum and any attempt to reduce *D* below 0.5 results in increase of solution concentration above 50%. This is explained more clearly later in Section 4.6.3. In the reverse parallel system, during T_{LPG} and T_{HPG} variation at (i) fixed $T_C = T_A$ =38°C and T_E =8°C and (ii) fixed $T_C = T_A$ =35°C and T_E =5°C however, the distribution ratios are taken as 0.6 and 0.65 respectively.

4.6.1 Effect of HPG temperature (T_{HPG}) on performance of double effect H_2O–LiCl VARS configurations

The effect of T_{HPG} variation on COP at three different absorber and condenser temperatures (33°C,35°C and 38°C) and two different evaporator temperatures (T_E =5°C and T_E =8°C) is shown in Fig. 4.4a and Fig. 4.4b. Fig. 4.4a corresponds to T_{HPG} variation with simultaneous change in T_{LPG} while in Fig. 4.4b, T_{HPG} variation is done for fixed T_{LPG} values. In Fig. 4.4a, during T_{HPG} variation from 95°C to 105°C (Case 1: fixed $T_C = T_A$ = 33°C and T_E = 8°C) with respect to the series flow configuration, a constant

34°C difference is maintained between T_{HPG} and T_{LPG}. In the parallel configuration, the T_{HPG} range is taken from 98°C to 106°C while in the reverse parallel configuration; the T_{HPG} range is small and it is varied from 100°C to 102°C. The difference between T_{HPG} and T_{LPG} in the parallel and reverse parallel systems are taken as 37°C and 39°C respectively. With temperatures fixed in the other components, the selected range of T_{HPG} variation for the series, parallel and reverse parallel configurations is clearly visible in Fig. 4.4a. At fixed $T_C = T_A$=35°C and T_E=8°C (Case 2), a difference of 36°C between T_{HPG} and T_{LPG} is maintained in the series configuration. For the parallel and reverse parallel systems, this difference between T_{HPG} and T_{LPG} are 38°C and 41°C respectively. At fixed $T_C = T_A$=38°C and T_E=8°C (Case 3), the difference between T_{HPG} and T_{LPG} is fixed at 40°C while for the parallel and reverse parallel systems, this difference between T_{HPG} and T_{LPG} are 41°C and 42°C respectively. At fixed $T_C = T_A$=35°C and T_E=5°C (Case 4), T_{HPG} and T_{LPG} difference is considered to be 39°C for the series configuration while in the parallel and reverse parallel systems, this differences are taken as 41°C and 42°C respectively. The decision regarding this simultaneous T_{HPG} and T_{LPG} change and also fixed T_{LPG} during T_{HPG} variation was taken after lot of maneuvering with the computer simulation programs to finally arrive at the optimal temperature difference in various cases.

From Fig. 4.4a, it was seen that the COP increases with increase in both T_{HPG} and T_{LPG} for all the three double effect system configurations at fixed other component temperatures. In the series configuration, during T_{HPG} variation from 95°C to 105°C (also T_{LPG} with 34°C difference) at fixed $T_C = T_A$=33°C and T_E=8°C, the maximum COP (1.428) was obtained at T_{HPG}=105°C and T_{LPG}=71°C.At fixed $T_C = T_A$=33°C and T_E =8°C, the maximum COP in the parallel configuration was found to be 1.469 which occurs at T_{HPG}=106°C and T_{LPG}=69°C. Similarly, in the reverse parallel configuration, the maximum COP (1.406) was found at T_{HPG}=102°C and T_{LPG}=63°C. Further it was seen that at a fixed T_E of 8°C, COP decreases with increasing absorber and condenser temperatures. The corresponding maximum COPs for Case 2 at $T_C = T_A$=35°C and T_E =

8°C for the series, parallel and reverse parallel systems were found 1.369, 1.411 and 1.347 respectively. These maximum COPs were obtained at T_{HPG} =109°C and T_{LPG} =73°C in the series configuration; T_{HPG} =109°C and T_{LPG} =71°C in the parallel configuration; T_{HPG} =108°C and T_{LPG}=67°C in the reverse parallel configuration. At T_C = T_A=38°C and T_E = 8°C, the maximum COPs were found to be 1.207, 1.273 and 1.209 respectively and these maximum COP values were obtained at T_{HPG} =116°C and T_{LPG} =76°C in the series configuration; T_{HPG} =116°C and T_{LPG} =75°C in the parallel configuration; T_{HPG} =115°C and T_{LPG} =73°C in the reverse parallel configuration. Comparing the performance of the double effects systems at fixed $T_C = T_A$=35°C and at two different evaporator temperatures, it was found that the double effect systems perform better at T_E =8°C than at T_E =5°C. It was also seen that the maximum COPs which were obtained for the double effect systems was the highest for the double effect parallel followed by those of the series and reverse parallel configurations.

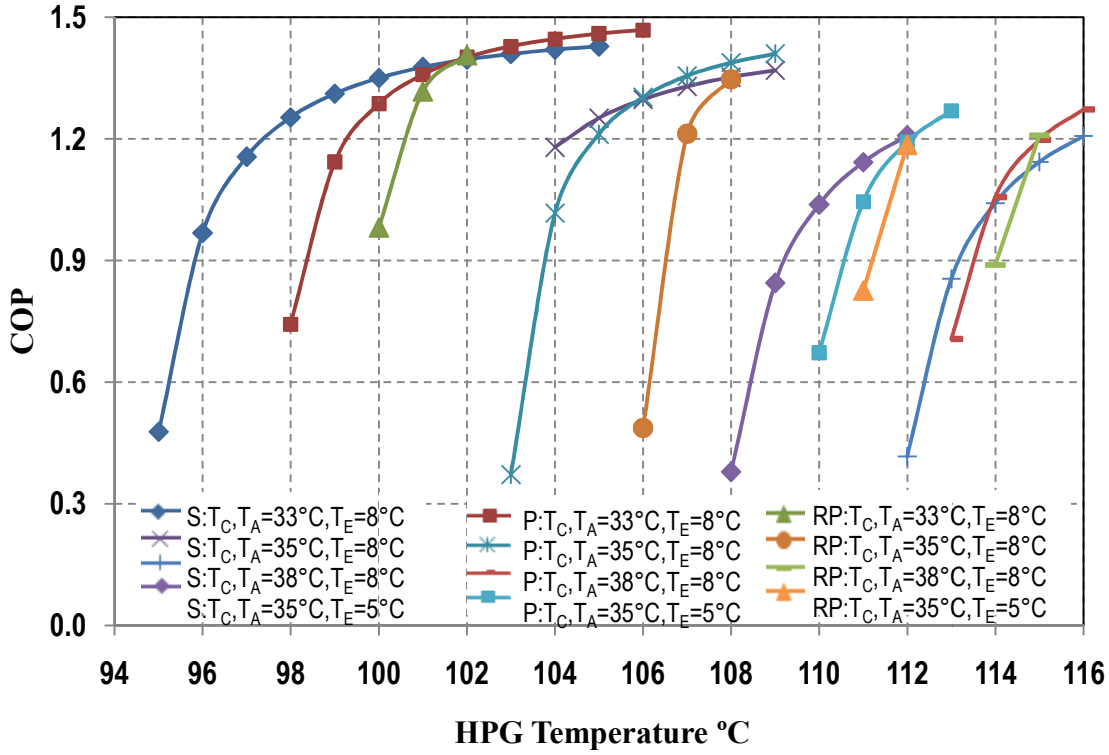

Fig 4.4a**:** COP **v**ariation with simultaneous change in T_{HPG} and T_{LPG} for the series, parallel and reverse parallel configurations with $T_{HPG} - T_{LPG}$ differences of (i) 34°C, 37°C and 39°C during Case 1, (ii) 36°C, 38°C and 41°C during Case 2 (iii) 40°C, 41°C and 42°C during Case 3 and (iv) 39°C, 41°C and 42°C during Case 4

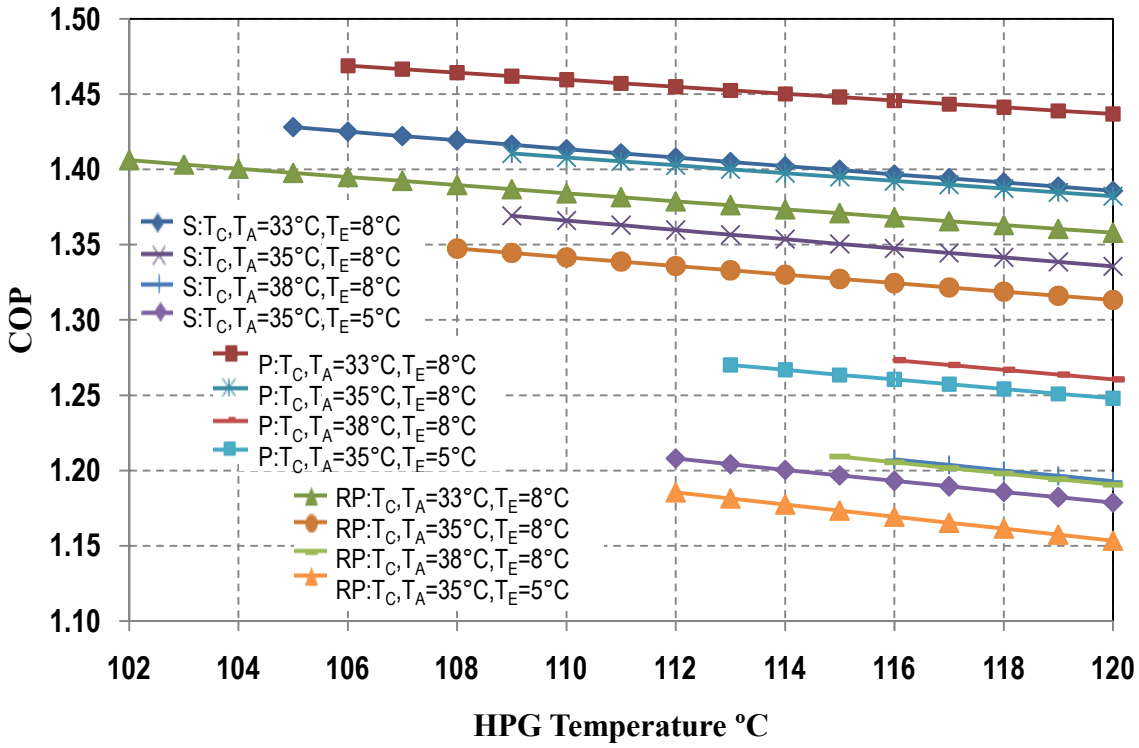

Fig 4.4b: COP variation with T_{HPG} at fixed T_{LPG} for the series, parallel and reverse parallel configurations respectively [T_{LPG} fixed at (i) 71°C, 69°C and 63°C during Case 1, (ii) 73°C, 71°C and 67°C during Case 2 (iii) 76°C, 75°C and 73°C during Case 3 (iv) 73°C, 72°C and 70°C during Case 4]

Further, it was observed that it is possible to operate the double effect H_2O–LiCl systems relatively at low T_{HPG} and T_{LPG}. The lower limit of T_{HPG} (and hence also T_{LPG}) is actually decided by the operating temperatures of the other components. The systems can be operated at low T_{HPG} by simultaneously lowering the absorber and condenser temperatures or alternately by increasing the evaporator temperature. Similarly, if the systems are to be operated at higher T_{HPG} and T_{LPG}, then this can be done by simultaneously increasing the absorber and condenser temperatures and lowering the evaporator temperature. The lower limit of T_{LPG} at fixed other component temperatures is actually limited by the mass balance in the system. It was earlier stated that the solution concentrations at the absorber, HPG and LPG outlets (X_4, X_8 and X_{15}) were determined by using a specific set of equations taken from Patek and Klomfar [3] through an iterative calculation**.** System operation of a given double effect system at T_{HPG} below certain limit leads to concentration values at which mass balance is no longer

satisfied. Say for example, X_4 in case of the series flow system must be less than X_{15} which is not satisfied when T_{HPG} is lowered below 95°C keeping T_C and T_A fixed at 33°C and T_E at 8°C (Fig. 4.4a). As mentioned earlier, X_4 and X_{15} calculations are done iteratively with known pressure and temperature in the absorber and LPG respectively. However, X_8 calculation is based on heat balance in the LPG (see Appendix for details). Therefore, at T_{HPG} below certain limit, X_{15} becomes less than X_4 and it affects the mass balance making system operation unrealistic.

It was also observed that the maximum solution concentration (X_{15}) in the series configuration is mainly controlled by T_{LPG} at fixed other components' temperatures. In the parallel and reverse parallel configurations, however, the maximum concentration (X_8) depends upon both T_{LPG} and the distribution ratio *D*. In Fig. 4.4a, during simultaneous T_{HPG} and T_{LPG} variation at fixed $T_C = T_A$=33°C and T_E=8°C (Case 1), the maximum limit of T_{LPG} was not allowed to exceed 71°C in the series configuration, 69°C in the parallel configuration and 63°C in the reverse parallel configuration. Similarly, at fixed $T_C = T_A$=35°C and T_E=8°C (Case 2), these maximum limits of T_{LPG} in the series, parallel and reverse parallel configurations were fixed at 71°C, 69°C and 63°C respectively. These upper T_{LPG} limits for the three double effect systems were 76°C., 75°C and 73°C at fixed $T_C = T_A$=38°C, T_E=8°C (Case 3). Accordingly, at fixed $T_C = T_A$ =35°C, T_E=5°C (Case 4) also, the maximum T_{LPG} limits were different for the three double effect VARS configuration. This was done because otherwise the maximum solution concentration (X_{15} in the series and X_8 in the parallel and reverse parallel) exceeds 50%. The changing solution concentrations (with simultaneous T_{HPG} and T_{LPG} variation) of the series, parallel and reverse parallel systems are shown in Table 4.5 (a–b) for all the four cases (Case 1–Case 4). That the maximum concentration in all these cases is within the limit of 0.5 is distinctly visible in Table 4.5 (a–b).

The pressure variation in the HPG is also shown in Table 4.5 (a–b) with simultaneous change in T_{HPG} and T_{LPG} for various test cases for all the three double effect systems. It was seen that for the series configuration, the HPG pressure (P_{HPG}) increases

with increase in T_{HPG} and T_{LPG} for all test cases while it decreases for the parallel and reverse parallel systems. The HPG pressure is dependent on T_{HPG} and X_8; since with simultaneous increase in T_{HPG} and T_{LPG}, X_8 also changes, therefore ultimately, the HPG pressure changes. The decreasing trend of P_{HPG} with simultaneous increase in T_{HPG} and T_{LPG} in the parallel and reverse parallel systems (as opposed to the series one) could be due to the distribution ratio *(D)* which is very crucial in these two systems as indicated earlier.

Since the evaporator temperature is the same (T_E=8°C) during Case 1, Case 2 and Case 3, therefore, the evaporator pressure (P_E) remains is the same (1.073 kPa) for all the three cases and it is also equal to the absorber pressure (P_A). During Case 4 at T_E =5°C, however, $P_E = P_A$=0.873 kPa. The evaporator and the absorber pressures are thus independent of change in T_C, T_A, T_{HPG} and T_{LPG}. Similarly the equal LPG and condenser pressures (P_{LPG} and P_C) are also shown in Table 4.5 (a–b) with respect to various test cases and these pressures don't change with T_E, T_A, T_{HPG} and T_{LPG}.

The corresponding results of heat loads in various system components and the SP power for all the three double effect H_2O–LiCl systems are shown in Table 4.6 (a–b). Heat load in the HPG ($\dot{Q}_{HPG}$) and SP power ($\dot{W}_{SP}$) decrease with simultaneous increase in T_{HPG} and T_{LPG} in all the three double effect VARS configurations. Therefore, COP shows a continuous increase with simultaneous increase in T_{HPG} and T_{LPG} in all the four cases. Absorber and condenser heat loads ($\dot{Q}_A$ and $\dot{Q}_C$) also decrease with simultaneous increase in T_{HPG} and T_{LPG}. LPG heat load ($\dot{Q}_{LPG}$) in the series configuration shows an increasing trend while the trend is opposite in the parallel and reverse parallel configurations. Depending on fixed temperatures in the other system components, since T_{LPG} cannot exceed beyond certain limit, therefore in Fig. 4.4b, the system performance (COP) variation is shown for the three double effect systems at T_{HPG} values higher than those presented in Fig. 4.4a, including also the last T_{HPG} value. However, here in Fig.

4.4b, T_{LPG} values are fixed at their corresponding limiting values with respect to the four different cases of fixed other components' temperatures.

Table 4.5a: Pressure and concentration variation with simultaneous T_{HPG} and T_{LPG} change

T_{HPG} (°C)	Series				Parallel					Reverse Parallel				
	P_{HPG} (kPa)	X_4	X_8	X_{15}	P_{HPG} (kPa)	X_4	X_8	X_{15}	X_{17}	P_{HPG} (kPa)	X_4	X_8	X_{15}	X_{17}
Case 1: $T_C = T_A = 33$°C, $T_E = 8$°C, $P_{LPG} = P_C = 5.035$ kPa, $P_A = P_E = 1.073$ kPa														
95	24.061	0.423	0.424	0.426		-	-	-	-		-	-	-	-
96	24.491	0.423	0.428	0.433		-	-	-	-		-	-	-	-
97	24.934	0.423	0.432	0.441		-	-	-	-		-	-	-	-
98	25.388	0.423	0.436	0.448	26.398	0.423	0.429	0.426	0.428		-	-	-	-
99	25.856	0.423	0.439	0.455	26.113	0.423	0.438	0.433	0.436		-	-	-	-
100	26.337	0.423	0.443	0.463	25.811	0.423	0.446	0.441	0.444	27.367	0.423	0.437	0.426	0.431
101	26.830	0.423	0.447	0.470	25.492	0.423	0.455	0.448	0.452	24.234	0.423	0.464	0.433	0.448
102	27.339	0.423	0.450	0.477	25.155	0.423	0.464	0.455	0.460	20.882	0.423	0.493	0.441	0.465
103	27.864	0.423	0.454	0.484	24.792	0.423	0.473	0.463	0.468		-	-	-	-
104	28.406	0.423	0.457	0.491	24.404	0.423	0.482	0.470	0.476		-	-	-	-
105	28.965	0.423	0.460	0.498	23.989	0.423	0.491	0.477	0.484		-	-	-	-
106		-	-	-	23.552	0.423	0.499	0.484	0.492		-	-	-	-
Case 2: $T_C = T_A = 35$°C, $T_E = 8$°C, $P_{LPG} = P_C = 5.629$ kPa, $P_A = P_E = 1.073$ kPa														
103		-	-	-	29.853	0.439	0.442	0.439	0.441		-	-	-	-
104	29.650	0.439	0.450	0.461	29.508	0.439	0.451	0.446	0.449		-	-	-	-
105	30.165	0.439	0.454	0.468	29.140	0.439	0.459	0.454	0.457		-	-	--	-
106	30.696	0.439	0.457	0.475	28.751	0.439	0.468	0.461	0.465	33.266	0.439	0.444	0.439	0.441
107	31.243	0.439	0.461	0.482	28.329	0.439	0.477	0.468	0.472	29.592	0.439	0.470	0.446	0.458
108	31.805	0.439	0.464	0.489	27.880	0.439	0.486	0.475	0.480	25.727	0.439	0.498	0.454	0.475
109	32.384	0.439	0.468	0.496	27.404	0.439	0.495	0.482	0.488					

Table 4.5b: Pressure and concentration variation with simultaneous T_{HPG} and T_{LPG} change

T_{HPG} (°C)	Series				Parallel					Reverse Parallel				
	P_{HPG} (kPa)	X_4	X_8	X_{15}	P_{HPG} (kPa)	X_4	X_8	X_{15}	X_{17}	P_{HPG} (kPa)	X_4	X_8	X_{15}	X_{17}
Case 3: $T_C = T_A = 38$°C, $T_E = 8$°C, $P_{LPG} = P_C = 6.632$ kPa, $P_A = P_E = 1.073$ kPa														
112	37.299	0.463	0.463	0.466		-	-	-	-		-	-	-	-
113	37.870	0.463	0.467	0.473	37.343	0.463	0.470	0.466	0.468		-	-	-	-
114	38.454	0.463	0.471	0.480	36.810	0.463	0.478	0.473	0.475	37.440	0.463	0.474	0.466	0.471
115	39.054	0.463	0.475	0.487	36.236	0.463	0.487	0.480	0.483	33.615	0.463	0.496	0.473	0.488
116	39.668	0.463	0.478	0.494	35.630	0.463	0.495	0.487	0.491		-	-	-	-
Case 4: $T_C = T_A = 35$°C, $T_E = 5$°C, $P_{LPG} = P_C = 5.629$ kPa, $P_A = P_E = 0.873$ kPa														
108	31.460	0.466	0.466	0.468		-	-	-	-		-	-	-	-
109	31.951	0.466	0.470	0.475		-	-	-	-		-	-	-	-
110	32.454	0.466	0.474	0.482	32.799	0.466	0.472	0.468	0.470		-	-	-	-
111	32.968	0.466	0.478	0.489	32.311	0.466	0.481	0.475	0.478	33.237	0.466	0.476	0.468	0.473
112	33.497	0.466	0.481	0.496	31.792	0.466	0.490	0.482	0.486	30.054	0.466	0.498	0.475	0.490
113		-	-	-	31.241	0.466	0.498	0.489	0.494		-	-	-	-

Table 4.6a: Variation of heat Loads ($\dot{Q}$ in kW) and SP powers ($\dot{W}_{SP1}$ and $\dot{W}_{SP2}$ in Watt) with simultaneous T_{HPG} and T_{LPG} change for Case 1 and Case 2

T_{HPG} (°C)	Series					Parallel					Reverse Parallel					
	$\dot{Q}_{HPG}$	$\dot{Q}_{LPG}$	$\dot{Q}_A$	$\dot{Q}_C$	$\dot{W}_{SP}$	$\dot{Q}_{HPG}$	$\dot{Q}_{LPG}$	$\dot{Q}_A$	$\dot{Q}_C$	$\dot{W}_{SP}$	$\dot{Q}_{HPG}$	$\dot{Q}_{LPG}$	$\dot{Q}_A$	$\dot{Q}_C$	$\dot{W}_{SP1}$	$\dot{W}_{SP2}$
	Case 1: $T_C = T_A = 33$°C, $T_E = 8$°C, $P_{LPG} = P_C = 5.035$ kPa, $P_A = P_E = 1.073$ kPa															
95	731.7	109.1	785.0	258.2	436.6	-	-	-	-	-	-	-	-	-	-	-
96	361.4	168.4	499.6	200.7	124.9	-	-	-	-	-	-	-	-	-	-	-
97	302.7	178.2	454.5	191.5	75.1	-	-	-	-	-	-	-	-	-	-	-
98	279.2	182.3	436.6	187.7	54.8	470.4	238.2	667.3	133.0	314.8	-	-	-	-	-	-
99	266.7	184.7	427.2	185.7	43.9	306.1	207.6	485.8	163.1	110.7	-	-	-	-	-	-
100	259.2	186.3	421.5	184.4	37.0	271.9	201.4	447.9	169.4	67.4	356.5	228.7	548.7	142.7	26.7	75.1
101	254.2	187.5	417.8	183.5	32.4	257.4	198.9	432.0	172.1	48.5	265.6	205.2	441.1	165.7	9.0	21.2
102	250.7	188.4	415.3	182.9	29.0	249.7	197.6	423.4	173.6	37.9	248.9	201.3	421.3	169.8	5.5	10.5
103	248.2	189.1	413.5	182.5	26.5	244.9	196.9	418.2	174.5	31.1	-	-	-	-	-	-
104	246.4	189.8	412.2	182.2	24.6	241.9	196.6	414.8	175.2	26.4	-	-	-	-	-	-
105	245.0	190.3	411.2	181.9	23.1	239.7	196.4	412.5	175.6	22.8	-	-	-	-	-	-
106	-	-	-	-	-	238.2	196.3	410.9	176.0	20.1						
	Case 2: $T_C = T_A = 35$°C, $T_E = 8$°C, $P_{LPG} = P_C = 5.629$ kPa, $P_A = P_E = 1.073$ kPa															
103	-	-	-	-	-	940.0	336.4	1192.1	39.0	954.6	-	-	-	-	-	-
104	296.7	182.2	451.4	189.3	74.2	343.8	217.0	528.4	155.2	164.2	-	-	-	-	-	-
105	279.6	185.1	438.2	186.8	57.8	288.7	206.2	467.0	166.0	90.1	-	-	-	-	-	-
106	269.6	186.9	430.6	185.2	47.9	268.5	202.3	444.4	170.1	62.2	717.5	329.0	979.5	46.9	102.6	313.8
107	263.2	188.2	425.6	184.3	41.4	258.1	200.4	432.9	172.2	47.4	288.4	212.4	467.2	160.2	13.6	35.4
108	258.8	189.2	422.3	183.6	36.9	252.0	199.4	426.1	173.4	38.3	259.7	205.0	433.1	167.6	7.4	15.9
109	255.6	190.0	419.9	183.1	33.5	248.1	198.8	421.7	174.3	32.2	-	-	-	-	-	-

Table 4.6b: Variation of heat Loads ($\dot{Q}$ in kW) and SP powers ($\dot{W}_{SP1}$ and $\dot{W}_{SP2}$ in Watt) with simultaneous T_{HPG} and T_{LPG} change for Case 3 and Case 4

T_{HPG} (°C)	Series					Parallel					Reverse Parallel					
	$\dot{Q}_{HPG}$	$\dot{Q}_{LPG}$	$\dot{Q}_A$	$\dot{Q}_C$	$\dot{W}_{SP}$	$\dot{Q}_{HPG}$	$\dot{Q}_{LPG}$	$\dot{Q}_A$	$\dot{Q}_C$	$\dot{W}_{SP}$	$\dot{Q}_{HPG}$	$\dot{Q}_{LPG}$	$\dot{Q}_A$	$\dot{Q}_C$	$\dot{W}_{SP1}$	$\dot{W}_{SP2}$
	Case 3: $T_C = T_A = 38$°C, $T_E = 8$°C, $P_{LPG} = P_C = 6.632$ kPa, $P_A = P_E = 1.073$ kPa															
112	838.8	106.6	877.2	264.3	696.0	-	-	-	-	-	-	-	-	-	-	-
113	409.2	168.6	540.4	204.5	211.2	494.8	250.3	697.6	125.2	414.4	-	-	-	-	-	-
114	335.9	179.4	483.0	194.3	128.1	331.0	216.4	514.1	158.4	161.5	393.6	236.1	584.4	139.2	36.1	120.2
115	305.9	184.0	459.6	190.1	93.8	292.0	208.5	470.3	166.3	100.4	289.4	211.5	463.2	163.2	13.1	37.4
116	289.8	186.6	447.0	187.9	75.1	274.8	205.1	451.1	169.9	72.9	-	-	-	-	-	-
	Case 4: $T_C = T_A = 35$°C, $T_E = 5$°C, $P_{LPG} = P_C = 5.629$ kPa, $P_A = P_E = 0.873$ kPa															
108	923.0	102.8	947.8	267.7	670.5	-	-	-	-	-	-	-	-	-	-	-
109	414.1	170.1	545.7	202.8	183.9	-	-	-	-	-	-	-	-	-	-	-
110	337.0	180.6	484.8	193.0	109.8	519.7	255.8	724.2	119.9	395.0	-	-	-	-	-	-
111	306.1	185.0	460.5	189.0	79.8	334.6	217.2	517.6	157.5	145.6	423.4	237.8	611.9	137.4	34.7	131.3
112	289.7	187.4	447.6	186.9	63.7	293.4	208.8	471.6	165.9	89.4	295.2	211.0	466.8	163.7	11.6	38.0
113	-	-	-	-	-	275.5	205.3	451.7	169.6	64.4	-	-	-	-	-	-

From Fig. 4.4b, it is seen that if T_{HPG} is increased further, keeping T_{LPG} fixed at their respective limiting values, COP of all the three double effect systems decreases. Therefore, it can now be said that the COPs which were shown earlier in Fig. 4.4a are the maximum at the respective values of T_{HPG} and T_{LPG}. During this T_{HPG} variation at fixed T_{LPG}, the solution concentrations don't change with T_{HPG} although the values are different in different test cases. The solution concentration values are shown in Table 4.7. Say for example in Case 1 at $T_C = T_A$=33°C and T_E=8°C, X_4 remains constant at 0.423 in all the three double effect systems. In the series configuration, X_8 and X_{15} remain fixed at 0.46 and 0.498 respectively.

In the parallel configuration, fixed X_8 and X_{15} values are 0.499 and 0.484 while in the reverse parallel configuration, these are respectively 0.492 and 0.441. It shows that the solution concentrations don't depend on T_{HPG} and hence the concentration values remain unchanged with increasing T_{HPG} at fixed T_{LPG}. Since, the concentration values don't change with T_{HPG} at fixed T_{LPG}, therefore, X_8 also remains invariant and consequently, the HPG pressure in the double effect systems increase when T_{HPG} increase. This is depicted in Fig. 4.5 for various test cases.

Corresponding to change in T_{HPG} at fixed T_{LPG}, the results concerning heat loads and SP power are shown in Table 4.8a for Case 1, Table 4.8b for Case 2 and Case 3 and in Table 4.8c for Case 4. COP decreases with further increase in T_{HPG} at fixed T_{LPG} for all the systems due to increase in HPG heat load ($\dot{Q}_{HPG}$) and SP power ($\dot{W}_{SP}$). In all the four cases, LPG heat load ($\dot{Q}_{LPG}$) decreases while condenser heat load ($\dot{Q}_C$) increases with T_{HPG} at fixed T_{LPG}. Absorber heat load ($\dot{Q}_A$) slightly increases in the parallel and reverse parallel configurations, which, however remains invariant with T_{HPG} in the series configuration.

Table 4.7: Fixed solution concentrations in various cases with respect to T_{HPG} variation at fixed T_{LPG}

Cases	Series			Parallel				Reverse Parallel			
	X_4	X_8	X_{15}	X_4	X_8	X_{15}	X_{17}	X_4	X_8	X_{15}	X_{17}
Case 1: $T_C = T_A = 33°C$, $T_E = 8°C$	0.423	0.460	0.498	0.423	0.499	0.484	0.492	0.423	0.492	0.441	0.465
Case 2: $T_C = T_A = 35°C$, $T_E = 8°C$	0.439	0.467	0.496	0.439	0.494	0.482	0.488	0.439	0.498	0.454	0.475
Case 3: $T_C = T_A = 38°C$, $T_E = 8°C$	0.463	0.478	0.494	0.463	0.495	0.487	0.491	0.463	0.496	0.473	0.487
Case 4: $T_C = T_A = 35°C$, $T_E = 5°C$	0.466	0.481	0.496	0.466	0.498	0.489	0.494	0.466	0.498	0.475	0.490

Table 4.8a: Variation of heat Loads ($\dot{Q}$ in kW) and SP powers ($\dot{W}_{SP1}$ and $\dot{W}_{SP2}$ in Watt) with T_{HPG} at fixed T_{LPG} for Case 1

T_{HPG} (°C)	Series					Parallel					Reverse Parallel					
	$\dot{Q}_{HPG}$	$\dot{Q}_{LPG}$	$\dot{Q}_A$	$\dot{Q}_C$	$\dot{W}_{SP}$	$\dot{Q}_{HPG}$	$\dot{Q}_{LPG}$	$\dot{Q}_A$	$\dot{Q}_C$	$\dot{W}_{SP}$	$\dot{Q}_{HPG}$	$\dot{Q}_{LPG}$	$\dot{Q}_A$	$\dot{Q}_C$	$\dot{W}_{SP1}$	$\dot{W}_{SP2}$
	Case 1: $T_C = T_A = 33$°C, $T_E = 8$°C, $P_{LPG} = P_C = 5.035$ kPa, $P_A = P_E = 1.073$ kPa															
102	-	-	-	-	-	-	-	-	-	-	248.9	201.3	421.3	169.8	5.47	10.5
103	-	-	-	-	-	-	-	-	-	-	249.4	201.1	421.4	170.2	5.47	11.1
104	-	-	-	-	-	-	-	-	-	-	249.9	200.8	421.5	170.5	5.47	11.7
105	245.0	190.3	411.2	181.9	23.1	-	-	-	-	-	250.4	200.6	421.6	170.9	5.48	12.3
106	245.5	189.9	411.2	182.4	24.0	238.2	196.3	410.9	176.0	20.1	250.9	200.4	421.7	171.3	5.48	13.0
107	246.1	189.6	411.2	182.9	25.0	238.6	196.2	410.9	176.2	20.9	251.4	200.2	421.9	171.6	5.48	13.7
108	246.6	189.3	411.2	183.4	26.1	239.0	196.1	411.0	176.5	21.8	251.8	200.0	422.0	172.0	5.48	14.3
109	247.1	188.9	411.2	183.8	27.1	239.4	195.9	411.1	176.8	22.7	252.3	199.7	422.1	172.4	5.48	15.1
110	247.6	188.6	411.2	184.3	28.2	239.8	195.8	411.2	177.1	23.7	252.8	199.5	422.2	172.7	5.49	15.8
111	248.1	188.2	411.2	184.8	29.4	240.1	195.6	411.3	177.4	24.6	253.3	199.3	422.3	173.1	5.49	16.6
112	248.6	187.9	411.2	185.3	30.6	240.5	195.5	411.3	177.7	25.6	253.8	199.1	422.4	173.5	5.49	17.4
113	249.1	187.6	411.2	185.7	31.8	240.9	195.4	411.4	177.9	26.7	254.3	198.8	422.6	173.8	5.49	18.2
114	249.5	187.2	411.2	186.2	33.0	241.3	195.2	411.5	178.2	27.8	254.8	198.6	422.7	174.2	5.50	19.0
115	250.0	186.9	411.2	186.7	34.3	241.7	195.1	411.6	178.5	28.9	255.3	198.4	422.8	174.6	5.50	19.9
116	250.5	186.5	411.2	187.2	35.7	242.0	195.0	411.7	178.8	30.0	255.8	198.2	422.9	175.0	5.50	20.8
117	251.0	186.2	411.2	187.6	37.1	242.4	194.8	411.8	179.1	31.2	256.3	197.9	423.0	175.3	5.50	21.8
118	251.5	185.8	411.2	188.1	38.5	242.8	194.7	411.8	179.4	32.4	256.7	197.7	423.2	175.7	5.50	22.7
119	252.0	185.5	411.2	188.6	40.0	243.2	194.5	411.9	179.6	33.6	257.2	197.5	423.3	176.1	5.51	23.7
120	252.5	185.2	411.2	189.1	41.5	243.5	194.4	412.0	179.9	34.9	257.7	197.3	423.4	176.4	5.51	24.8

Table 4.8b: Variation of heat Loads ($\dot{Q}$ in kW) and SP powers ($\dot{W}_{SP1}$ and $\dot{W}_{SP2}$ in Watt) with T_{HPG} at fixed T_{LPG} for Case 2 and Case 3

T_{HPG} (°C)	Series					Parallel					Reverse Parallel					
	$\dot{Q}_{HPG}$	$\dot{Q}_{LPG}$	$\dot{Q}_A$	$\dot{Q}_C$	$\dot{W}_{SP}$	$\dot{Q}_{HPG}$	$\dot{Q}_{LPG}$	$\dot{Q}_A$	$\dot{Q}_C$	$\dot{W}_{SP}$	$\dot{Q}_{HPG}$	$\dot{Q}_{LPG}$	$\dot{Q}_A$	$\dot{Q}_C$	$\dot{W}_{SP1}$	$\dot{W}_{SP2}$
	Case 2: $T_C = T_A = 35°C$, $T_E = 8°C$, $P_{LPG} = P_C = 5.629$ kPa, $P_A = P_E = 1.073$ kPa															
108	-	-	-	-	-	-	-	-	-	-	259.7	205.0	433.1	167.6	7.44	15.9
109	255.6	190.0	419.9	183.1	33.5	248.1	198.8	421.7	174.3	32.2	260.3	204.8	433.2	168.0	7.44	16.7
110	256.2	189.6	419.9	183.7	34.8	248.5	198.7	421.8	174.6	33.5	260.8	204.5	433.4	168.4	7.45	17.5
111	256.8	189.1	419.9	184.2	36.2	249.0	198.5	422.0	174.9	34.9	261.4	204.3	433.5	168.8	7.45	18.4
112	257.3	188.7	419.9	184.8	37.7	249.5	198.3	422.1	175.2	36.3	262.0	204.0	433.7	169.2	7.46	19.3
113	257.9	188.3	419.9	185.4	39.2	249.9	198.2	422.2	175.5	37.8	262.5	203.8	433.8	169.6	7.46	20.3
114	258.5	187.9	419.9	185.9	40.8	250.4	198.0	422.3	175.9	39.3	263.1	203.5	434.0	170.0	7.46	21.3
115	259.1	187.4	419.9	186.5	42.4	250.9	197.8	422.5	176.2	40.9	263.7	203.3	434.1	170.4	7.47	22.3
116	259.7	187.0	419.9	187.0	44.1	251.3	197.7	422.6	176.5	42.5	264.2	203.0	434.3	170.8	7.47	23.4
117	260.3	186.6	419.9	187.6	45.8	251.8	197.5	422.7	176.8	44.2	264.8	202.8	434.4	171.2	7.48	24.4
118	260.8	186.2	419.9	188.1	47.5	252.2	197.3	422.8	177.1	45.9	265.3	202.5	434.6	171.6	7.48	25.6
119	261.4	185.7	419.9	188.7	49.4	252.7	197.2	423.0	177.4	47.7	265.9	202.2	434.7	172.0	7.49	26.7
120	262.0	185.3	419.9	189.2	51.3	253.1	197.0	423.1	177.7	49.5	266.5	202.0	434.9	172.4	7.49	27.9
	Case 3: $T_C = T_A = 38°C$, $T_E = 8°C$, $P_{LPG} = P_C = 6.632$ kPa, $P_A = P_E = 1.073$ kPa															
115	-	-	-	-	-	-	-	-	-	-	289.4	211.5	463.2	163.2	13.1	37.4
116	289.8	186.6	447.0	187.9	75.1	274.8	205.1	451.1	169.9	72.9	290.3	211.2	463.5	163.8	13.1	39.3
117	290.7	185.9	447.0	188.7	78.1	275.5	204.9	451.3	170.3	75.8	291.2	210.8	463.9	164.3	13.1	41.2
118	291.6	185.2	447.0	189.6	81.1	276.2	204.6	451.6	170.7	78.8	292.1	210.4	464.2	164.8	13.1	43.2
119	292.5	184.5	447.0	190.4	84.2	276.9	204.4	451.8	171.0	81.9	293.0	210.0	464.6	165.4	13.2	45.3
120	293.3	183.8	447.0	191.2	87.5	277.6	204.1	452.1	171.4	85.1	293.9	209.6	464.9	165.9	13.2	47.4

Table 4.8c: Variation of heat Loads ($\dot{Q}$ in kW) and SP powers ($\dot{W}_{SP1}$ and $\dot{W}_{SP2}$ in Watt) with T_{HPG} at fixed T_{LPG} for Case 4

T_{HPG} (°C)	Series					Parallel					Reverse Parallel					
	$\dot{Q}_{HPG}$	$\dot{Q}_{LPG}$	$\dot{Q}_A$	$\dot{Q}_C$	$\dot{W}_{SP}$	$\dot{Q}_{HPG}$	$\dot{Q}_{LPG}$	$\dot{Q}_A$	$\dot{Q}_C$	$\dot{W}_{SP}$	$\dot{Q}_{HPG}$	$\dot{Q}_{LPG}$	$\dot{Q}_A$	$\dot{Q}_C$	$\dot{W}_{SP1}$	$\dot{W}_{SP2}$
	Case 4: $T_C = T_A = 35°C$, $T_E = 5°C$, $P_{LPG} = P_C = 5.629$ kPa, $P_A = P_E = 0.873$ kPa															
112	289.7	187.4	447.6	186.9	63.7	-	-	-	-	-	295.2	211.0	466.8	163.7	11.6	38.0
113	290.6	186.7	447.6	187.7	66.3	275.5	205.3	451.7	169.6	64.4	296.2	210.6	467.2	164.3	11.6	39.9
114	291.5	186.0	447.6	188.6	68.9	276.2	205.1	451.9	170.0	67.1	297.2	210.1	467.6	164.9	11.6	41.9
115	292.4	185.2	447.6	189.4	71.7	276.9	204.8	452.2	170.4	69.8	298.3	209.7	468.0	165.4	11.6	43.9
116	293.3	184.5	447.5	190.3	74.5	277.6	204.6	452.5	170.8	72.6	299.3	209.3	468.4	166.0	11.6	46.1
117	294.2	183.8	447.5	191.1	77.4	278.3	204.3	452.7	171.2	75.5	300.3	208.9	468.8	166.6	11.7	48.3
118	295.1	183.1	447.5	192.0	80.4	279.0	204.1	453.0	171.6	78.5	301.3	208.4	469.2	167.1	11.7	50.6
119	296.0	182.4	447.5	192.8	83.5	279.7	203.9	453.3	172.0	81.6	302.3	208.0	469.6	167.7	11.7	52.9
120	296.9	181.6	447.5	193.7	86.7	280.4	203.6	453.5	172.4	84.8	303.4	207.6	470.0	168.3	11.7	55.4

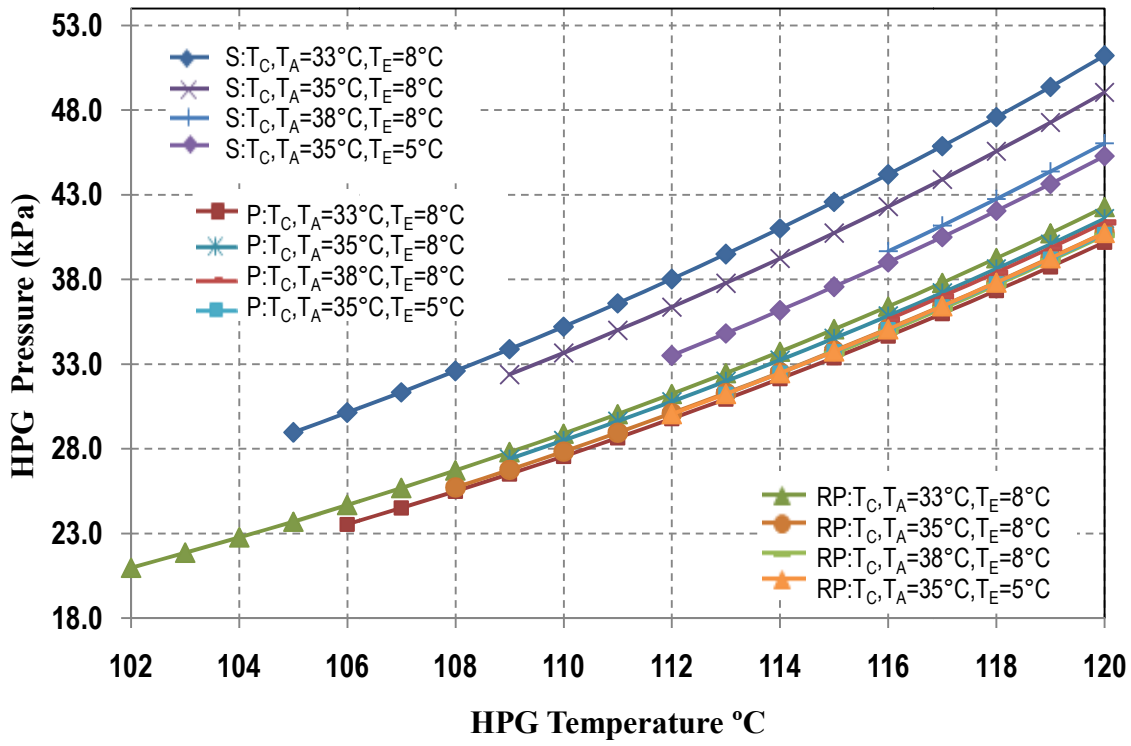

Fig 4.5: P_{HPG} variation with T_{HPG} at fixed T_{LPG} for the series, parallel and reverse parallel configurations respectively [T_{LPG} fixed at (i) 71°C, 69°C and 63°C during Case 1, (ii) 73°C, 71°C and 67°C during Case 2 iii) 76°C, 75°C and 73°C during Case 3 (iv) 73°C, 72°C and 70°C during Case 4]

4.6.2 Effect of LPG temperature (T_{HPG}) on performance of double effect H_2O–LiCl VARS configurations

Earlier in Fig. 4.4a and Fig. 4.4b, when COP was shown corresponding to (i) simultaneous T_{HPG} and T_{LPG} variation and (ii) T_{HPG} variation at fixed T_{LPG}, it was found that for a given test case, there exists an optimal T_{HPG} and T_{LPG} combination at which the COPs of the respective double effect H_2O–LiCl systems are maximum. During simultaneous T_{HPG} and T_{LPG} variation, the difference between the two were so selected (after running the computer programs several times with various temperature differences between T_{HPG} and T_{LPG} and finally selecting the one that was reported earlier) that the COP value that was obtained is ultimately a maximum COP value within that range. The limiting upper T_{LPG} (the value at which maximum solution concentration is within the limit of 0.5) was also found out earlier for all the three systems for various test cases.

Here in Fig. 4.6, COP is now shown for all the systems with changing T_{LPG} at the corresponding fixed optimum T_{HPG} values to establish the fact regarding maximum COP and the corresponding optimal T_{HPG} and T_{LPG} values for all the cases.

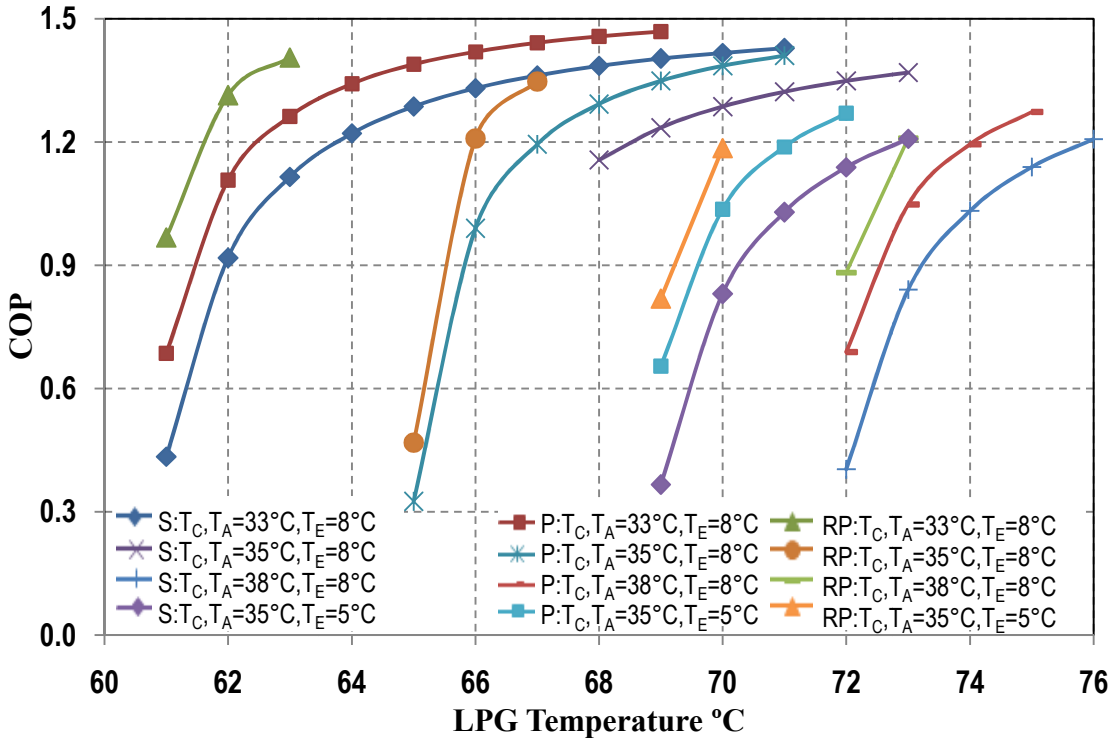

Fig 4.6: COP variation with T_{LPG} at fixed T_{HPG} for the series, parallel and reverse parallel configurations respectively [T_{HPG} fixed at (i) 105°C, 106°C and 102°C during Case 1, (ii) 109°C, 109°C and 108°C during Case 2 (iii) 116°C, 116°C and 115°C during Case 3 (iv) 112°C, 113°C and 112°C during Case 4]

Say for example, in Case 1 at $T_C = T_A$=33°C and T_E=8°C, the T_{HPG} values for the series, parallel and reverse parallel systems were fixed at 105°C, 106°C and 102°C and accordingly, T_{LPG} was increased to its maximum possible value (limited by 50% solution concentration) to show the occurrence of maximum COP at those T_{HPG} and T_{LPG} values that were obtained earlier. This COP variation is additionally shown in Fig. 4.6 because earlier in Fig. 4.4a, it was shown for a constant temperature difference between T_{HPG} and T_{LPG}. From Fig. 4.6, it is now seen that COP increases with T_{LPG} at fixed T_{HPG} for all the systems in various test cases. However, T_{LPG} cannot cross the upper limit set by the maximum solution concentration of 50%. T_{LPG} also has a lower limit set by the mass

balance due to non fulfillment of previously mentioned criteria of concentration values. This is the reason that the range of T_{LPG} was very narrow for the reverse parallel systems in all the test cases.

At fixed T_{HPG}, the HPG pressure (P_{HPG}) decreases with increase in T_{LPG} in all the three double effect VARS configurations at various test cases. Say for example during Case 1, P_{HPG} decreases from 35.909 kPa at T_{LPG}=61°C to 28.964 kPa at T_{LPG}=71°C in the series configuration. Similarly, in the reverse parallel system, during Case 1, P_{HPG} decreases from 36.262 kPa at T_{LPG}=61°C to 23.552 kPa at T_{LPG}=69°C Actually with increase in T_{LPG} at fixed T_{HPG}, X_8 increases and since P_{HPG} is a function of X_8 and T_{HPG}, therefore, it finally results in decrease of P_{HPG} at higher T_{LPG}.

The component heat loads and SP power with respect to T_{LPG} variation at fixed T_{HPG} for various test cases is shown in Table 4.9(a–b). With T_{HPG} fixed at their respective optimal values, when T_{LPG} is increased up to the maximum limit, HPG heat load ($\dot{Q}_{HPG}$) and SP power ($\dot{W}_{SP}$) decreases leading to COP increase in all the four test cases. In all the four various cases, $\dot{Q}_{LPG}$ increases while $\dot{Q}_A$ and $\dot{Q}_C$ decrease with T_{LPG} in the series configuration. On the other hand, in the parallel and reverse parallel configurations, both $\dot{Q}_{LPG}$ and $\dot{Q}_A$ decrease while $\dot{Q}_C$ increases with increase in T_{LPG}.

4.6.3 Effect of *D* on performance of the double effect parallel and reverse parallel H_2O–LiCl systems

The effect of distribution ratio *'D'* on performance (COP) of the double effect parallel and reverse parallel configurations is shown in Fig. 4.7. It was seen that the COP of both the parallel and reverse parallel systems decreases with increase in *D* in all the cases. *D* cannot be lowered below certain value in the parallel and reverse parallel systems because the solution concentration at HPG exit (X_8) in that case exceeds 50%. In the parallel system, the lower *D* limit was found to be 0.5 in Case 1 ($T_C = T_A$=33°C and T_E=8°C), Case 2 ($T_C = T_A$=35°C and T_E=8°C) and Case 3 ($T_C = T_A$=38°C and T_E =8°C).

Table 4.9a: Variation of heat Loads ($\dot{Q}$ in kW) and SP powers ($\dot{W}_{SP1}$ and $\dot{W}_{SP2}$ in Watt) with T_{LPG} at fixed T_{HPG} for Case 1 and case 2

T_{LPG} (°C)	Series					Parallel					Reverse Parallel					
	$\dot{Q}_{HPG}$	$\dot{Q}_{LPG}$	$\dot{Q}_A$	$\dot{Q}_C$	$\dot{W}_{SP}$	$\dot{Q}_{HPG}$	$\dot{Q}_{LPG}$	$\dot{Q}_A$	$\dot{Q}_C$	$\dot{W}_{SP}$	$\dot{Q}_{HPG}$	$\dot{Q}_{LPG}$	$\dot{Q}_A$	$\dot{Q}_C$	$\dot{W}_{SP1}$	$\dot{W}_{SP2}$
	Case 1: $T_C = T_A = 33$°C, $T_E = 8$°C, $P_{LPG} = P_C = 5.035$ kPa, $P_A = P_E = 1.073$ kPa															
61	805.2	41.0	785.0	324.8	661.6	509.9	230.9	694.7	141.6	459.1	361.5	227.1	551.5	144.5	26.9	83.5
62	381.2	150.9	499.6	218.9	181.6	316.0	204.6	490.8	167.1	149.6	266.4	204.9	441.3	166.2	9.0	22.3
63	313.8	168.8	454.5	201.7	104.7	277.1	199.6	450.2	172.0	86.8	248.9	201.3	421.3	169.8	5.5	10.5
64	286.5	176.4	436.6	194.5	73.3	260.8	197.7	433.2	174.0	59.8	-	-	-	-	-	-
65	271.9	180.7	427.2	190.5	56.3	251.9	196.8	424.2	175.0	44.8	-	-	-	-	-	-
66	262.9	183.5	421.5	187.9	45.6	246.4	196.4	418.7	175.5	35.3	-	-	-	-	-	-
67	256.8	185.5	417.8	186.0	38.2	242.7	196.2	415.1	175.8	28.6	-	-	-	-	-	-
68	252.5	187.1	415.3	184.6	32.9	240.1	196.2	412.6	175.9	23.8	-	-	-	-	-	-
69	249.4	188.4	413.5	183.5	28.8	238.2	196.3	410.9	176.0	20.1	-	-	-	-	-	-
70	246.9	189.4	412.2	182.7	25.6	-	-	-	-	-	-	-	-	-	-	-
71	245.0	190.3	411.2	181.9	23.1	-	-	-	-	-	-					
	Case 2: $T_C = T_A = 35$°C, $T_E = 8$°C, $P_{LPG} = P_C = 5.629$ kPa, $P_A = P_E = 1.073$ kPa															
65	-	-	-	-	-	1075	332	1311	44.2	1352	746.6	327.6	1004.3	48.8	106.2	356.4
66	-	-	-	-	-	353.2	214.4	533.7	158.6	203.5	289.4	212.0	467.6	160.8	13.7	37.2
67	-	-	-	-	-	292.8	204.8	468.8	168.0	106.4	259.7	205.0	433.1	167.6	7.4	15.9
68	302.5	177.4	451.4	194.7	90.9	270.7	201.5	445.3	171.3	70.3	-	-	-	-	-	-
69	283.3	182.1	438.2	190.2	67.9	259.3	200.0	433.3	172.9	51.5	-	-	-	-	-	-
70	272.0	185.1	430.6	187.5	54.1	252.6	199.2	426.3	173.8	39.9	-	-	-	-	-	-
71	264.6	187.2	425.6	185.6	44.9	248.1	198.8	421.7	174.3	32.2	-	-	-	-	-	-
72	259.4	188.7	422.3	184.2	38.4	-	-	-	-	-	-	-	-	-	-	-
73	255.6	190.0	419.9	183.1	33.5	-	-	-	-	-	-	-	-	-	-	-

Table 4.9b: Variation of heat Loads ($\dot{Q}$ in kW) and SP powers ($\dot{W}_{SP1}$ and $\dot{W}_{SP2}$ in Watt) with T_{LPG} at fixed T_{HPG} for Case 3 and case 4

T_{LPG} (°C)	Series					Parallel					Reverse Parallel					
	$\dot{Q}_{HPG}$	$\dot{Q}_{LPG}$	$\dot{Q}_A$	$\dot{Q}_C$	$\dot{W}_{SP}$	$\dot{Q}_{HPG}$	$\dot{Q}_{LPG}$	$\dot{Q}_A$	$\dot{Q}_C$	$\dot{W}_{SP}$	$\dot{Q}_{HPG}$	$\dot{Q}_{LPG}$	$\dot{Q}_A$	$\dot{Q}_C$	$\dot{W}_{SP1}$	$\dot{W}_{SP2}$
	Case 3: $T_C = T_A = 38°C$, $T_E = 8°C$, $P_{LPG} = P_C = 6.632$ kPa, $P_A = P_E = 1.073$ kPa															
72	867.1	79.8	877.2	290.5	812.9	507.9	248.0	707.0	128.0	473.2	396.5	235.2	586.1	140.2	36.3	126.6
73	416.0	162.4	540.4	210.8	237.3	333.9	215.6	515.6	159.5	175.2	289.4	211.5	463.2	163.2	13.1	37.4
74	338.7	176.9	483.0	197.0	138.4	292.9	208.2	470.7	166.8	104.5	-	-	-	-	-	-
75	307.0	183.1	459.6	191.1	97.5	274.8	205.1	451.1	169.9	72.9	-	-	-	-	-	-
76	289.8	186.6	447.0	187.9	75.1	-	-	-	-	-	-	-	-	-	-	-
	Case 4: $T_C = T_A = 35°C$, $T_E = 5°C$, $P_{LPG} = P_C = 5.629$ kPa, $P_A = P_E = 0.873$ kPa															
69	956.0	72.2	947.8	297.6	786.1	534.4	253.4	734.7	122.7	452.5	427.2	236.9	614.2	138.6	34.9	138.5
70	421.2	163.8	545.7	209.3	207.2	337.5	216.4	519.1	158.6	158.1	295.2	211.0	466.8	163.7	11.6	38.0
71	340.0	178.1	484.8	195.7	118.9	294.3	208.5	472.1	166.4	93.1	-	-	-	-	-	-
72	307.2	184.1	460.5	190.0	83.1	275.5	205.3	451.7	169.6	64.4	-	-	-	-	-	-
73	289.7	187.4	447.6	186.9	63.7	-	-	-	-	-	-	-	-	-	-	-

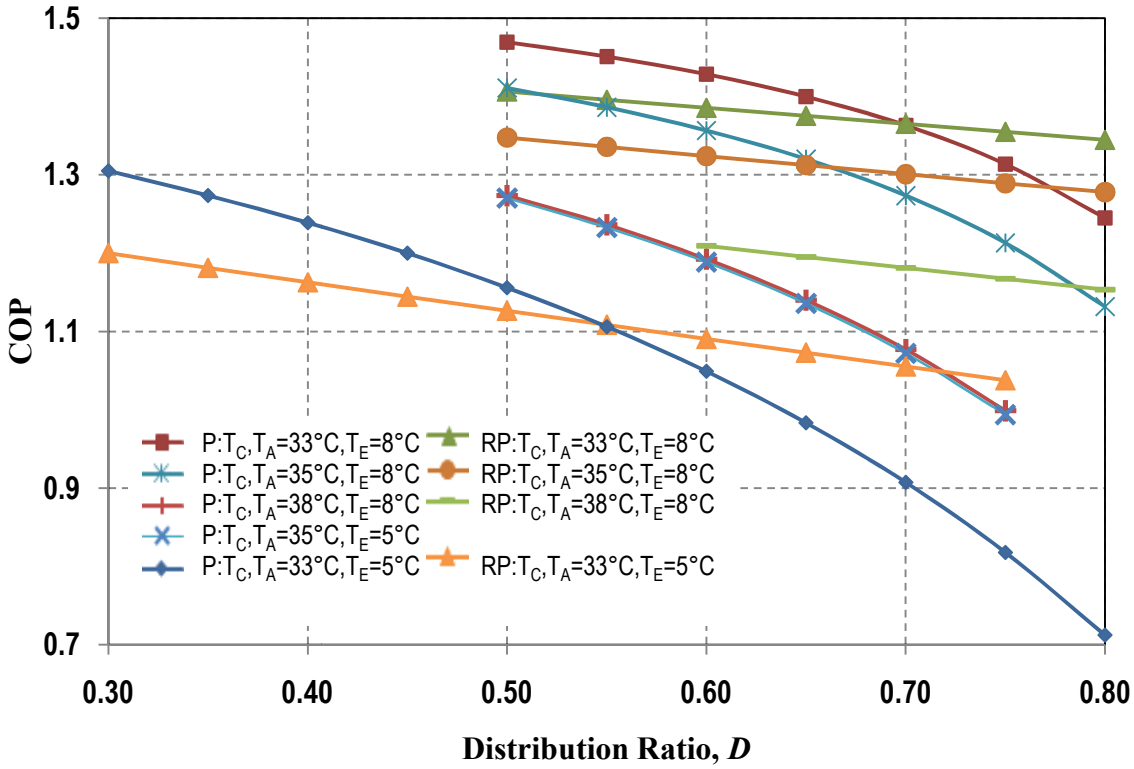

Fig 4.7: COP variation with distribution ratio (D) at fixed T_{HPG} and T_{LPG} for the parallel and reverse parallel configurations respectively [(i) T_{HPG} fixed at 106°C and 102°C; T_{LPG} fixed at 69°C and 63°C during Case 1, (ii) T_{HPG} fixed at 109°C and 108°C; T_{LPG} fixed at 71°C and 67°C during Case 2, (iii) T_{HPG} fixed at 116°C and 115°C; T_{LPG} fixed at 75°C and 73°C during Case 3, (iv) T_{HPG} fixed at 113°C and T_{LPG} fixed at 72 for the parallel system during Case 4 (v) T_{HPG} fixed at 106°C and 104°C; T_{LPG} fixed at 66°C and 65°C during the additional case (Case 5: $T_C = T_A = 33$°C, $T_E = 5$°C)]

Similarly in the reverse parallel system also, the lower D limit was found 0.5 for Case 1 and Case 2. However, in Case 3, the lower D limit of the reverse parallel system was found 0.6. Not much D variation was possible in the reverse parallel system in Case 4 ($T_C = T_A$=35°C and T_E=5°C), hence COP variation with D is not shown and the lower D limit for this case was found 0.65. However, when $T_C = T_A$=33°C and T_E=5°C, D can be lowered up to 0.3 in both the parallel and reverse parallel systems and this case is now additionally shown in Fig. 4.7. It was also found that there exists a certain range of D values at which the COP of the parallel system is more compared to that of the reverse parallel system and vice versa.

The solution concentrations with changing D for all these cases are shown in Table 4.10. It is seen that that the maximum solution concentrations (X_8 in the parallel and reverse parallel) occur when D is in its lower limit in all the cases and increase in D causes reduction in maximum concentration values.

Table 4.10: Pressure and concentration variation with D of the double effect parallel and reverse parallel systems

D	Parallel					Reverse Parallel				
	P_{HPG} (kPa)	X_4	X_8	X_{15}	X_{17}	P_{HPG} (kPa)	X_4	X_8	X_{15}	X_{17}
Case 1: $T_C = T_A = 33°C$, $T_E = 8°C$, $P_{LPG} = P_C = 5.035$ kPa, $P_A = P_E = 1.073$ kPa										
0.50	23.552	0.423	0.499	0.484	0.492	20.982	0.423	0.493	0.441	0.465
0.60	28.219	0.423	0.471	0.484	0.476	22.380	0.423	0.483	0.441	0.465
0.70	31.540	0.423	0.453	0.484	0.462	23.383	0.423	0.476	0.441	0.465
0.80	34.011	0.423	0.440	0.484	0.448	24.138	0.423	0.471	0.441	0.464
Case 2: $T_C = T_A = 35°C$, $T_E = 8°C$, $P_{LPG} = P_C = 5.629$ kPa, $P_A = P_E = 1.073$ kPa										
0.50	27.404	0.439	0.495	0.482	0.488	25.727	0.439	0.498	0.454	0.475
0.60	31.129	0.439	0.474	0.482	0.478	27.199	0.439	0.490	0.454	0.475
0.70	33.763	0.439	0.461	0.482	0.467	28.255	0.439	0.484	0.454	0.474
0.80	35.712	0.439	0.451	0.482	0.457	29.048	0.439	0.479	0.454	0.474
Case 3: $T_C = T_A = 38°C$, $T_E = 8°C$, $P_{LPG} = P_C = 6.632$ kPa, $P_A = P_E = 1.073$ kPa										
0.50	35.630	0.463	0.495	0.487	0.491		-	-	-	-
0.60	38.355	0.463	0.484	0.487	0.485	33.615	0.463	0.499	0.473	0.488
0.70	40.273	0.463	0.476	0.487	0.479	34.589	0.463	0.494	0.473	0.488
0.75	41.028	0.463	0.473	0.487	0.476	34.979	0.463	0.492	0.473	0.487
0.80		-	-	-	-	35.321	0.463	0.491	0.473	0.487
Additional case (**Case 5**) : $T_C = T_A = 33°C$, $T_E = 5°C$, $P_{LPG} = P_C = 5.035$ kPa, $P_A = P_E = 0.873$ kPa										
0.30	23.967	0.450	0.497	0.463	0.472	22.957	0.450	0.491	0.455	0.466
0.40	26.947	0.450	0.479	0.463	0.469	24.532	0.450	0.481	0.455	0.465
0.50	28.731	0.450	0.468	0.463	0.465	25.480	0.450	0.475	0.455	0.465
0.60	29.909	0.450	0.462	0.463	0.462	26.113	0.450	0.471	0.455	0.465
0.70	30.738	0.450	0.457	0.463	0.459	26.566	0.450	0.468	0.455	0.464
0.80	31.344	0.450	0.454	0.463	0.456	26.907	0.450	0.466	0.455	0.464

Further, the HPG pressure also increases with *D* at various cases in both the double effect parallel and reverse parallel systems. This is mainly due to reduction in X_8 at higher *D* that occurs in both the parallel and reverse parallel systems in all the test cases. Earlier with T_{LPG} variation at fixed T_{HPG}, it was observed that when X_8 increases, simultaneously P_{HPG} also reduces. Now since with increase in *D*, X_8 decreases, therefore it causes increase in P_{HPG}.

Weak and strong solution concentrations are not affected by *D* variation. This is because, the strong solution concentration (X_4) at absorber exit is a function of absorber pressure and temperature while the weak strong solution concentration at LPG exit (X_{15}) depends on LPG pressure and LPG temperature. These are not related and have nothing to do with the distribution ratio *D* because distribution ratio *D* in no way affects the pressure and temperature in the absorber and the LPG. Absorber and LPG temperatures are input model parameters. The absorber pressure is set equal to the evaporator pressure and thus it is the saturation pressure of water (refrigerant) corresponding to evaporator temperature. Similarly, the LPG pressure is set equal to condenser pressure and it is the saturation pressure of water (refrigerant) corresponding to condenser temperature.

Component heat loads and SP power corresponding to *D* variation are shown in Table 4.11. With increase in *D*, $\dot{Q}_{HPG}$ and $\dot{W}_{SP}$ increase in both the parallel and reverse parallel double effect systems at various test cases and therefore COP decreases with increase in *D*. In the double effect parallel configuration, with increase in *D*, the mass flow rate of strong solution entering the HPG ($\dot{m}_7$) increases while the flow rate of primary vapour generated in the HPG ($\dot{m}_{11}$) slightly reduces. Due to this reason, the mass flow rate of HPG leaving medium solution ($\dot{m}_8$) also shows a proportionate increase in its value. Increase in *D* also causes an increase in the temperature of the strong solution at state 7. The pressure at state 7 also increases due to increase in P_{HPG} with *D*. With concentration remaining constant but due to change in temperature and pressure, finally the specific enthalpy at state 7 (h_7) increases from 253.982 kJ/kg at *D*=0.5 to 273.456 kJ/kg at *D*=0.8 during Case 1 at $T_C = T_A$=33°C and T_E=8°C. On the

other hand, the specific enthalpy at state 8 (h_8) decreases from 345.167 kJ/kg at *D*=0.5 to 315.7 kJ/kg at *D*=0.8; mainly due to increase in P_{HPG} and reduction in X_8.

Table 4.11: Heat Load and SP power variation with D

D	Parallel					Reverse Parallel					
	$\dot{Q}_{HPG}$	$\dot{Q}_{LPG}$	$\dot{Q}_A$	$\dot{Q}_C$	$\dot{W}_{SP}$	$\dot{Q}_{HPG}$	$\dot{Q}_{LPG}$	$\dot{Q}_A$	$\dot{Q}_C$	$\dot{W}_{SP1}$	$\dot{W}_{SP2}$
Case 1: $T_C = T_A = 33°C$, $T_E = 8°C$, $P_{LPG} = P_C = 5.035$ kPa, $P_A = P_E = 1.073$ kPa											
0.50	238.2	196.3	410.9	176.0	20.1	248.9	201.3	421.3	169.8	5.5	10.5
0.60	245.0	194.9	415.6	177.4	30.3	252.6	199.9	422.3	171.1	5.5	13.8
0.70	256.8	193.5	424.9	178.7	45.6	256.4	198.6	423.4	172.4	5.5	17.2
0.80	281.1	192.0	445.8	180.1	74.3	260.3	197.2	424.6	173.7	5.6	20.6
Case 2: $T_C = T_A = 35°C$, $T_E = 8°C$, $P_{LPG} = P_C = 5.629$ kPa, $P_A = P_E = 1.073$ kPa											
0.50	248.1	198.8	421.7	174.3	32.2	259.7	205.0	433.1	167.6	7.4	15.9
0.60	258.0	197.4	429.4	175.6	46.0	264.4	203.3	434.5	169.3	7.5	20.6
0.70	274.8	196.1	443.4	177.0	67.0	269.1	201.7	436.1	170.8	7.6	25.4
0.80	309.2	194.6	473.5	178.4	107.1	273.9	200.1	437.6	172.4	7.6	30.3
Case 3: $T_C = T_A = 38°C$, $T_E = 8°C$, $P_{LPG} = P_C = 6.632$ kPa, $P_A = P_E = 1.073$ kPa											
0.50	274.8	205.1	451.1	169.9	72.9	-	-	-	-	-	-
0.60	293.5	203.6	466.7	171.3	98.8	289.4	211.5	463.2	163.2	13.1	37.4
0.70	324.9	202.0	494.1	172.9	139.6	296.3	209.2	465.9	165.5	13.3	45.9
0.75	350.3	201.1	516.6	173.7	171.5	299.8	208.1	467.4	166.6	13.4	50.2
0.80	-	-	-	-	-	303.4	206.9	468.8	167.7	13.5	54.6
Additional case (**Case 5**): $T_C = T_A = 33°C$, $T_E = 5°C$, $P_{LPG} = P_C = 5.035$ kPa, $P_A = P_E = 0.873$ kPa											
0.30	268.2	212.2	453.1	161.0	58.5	287.2	226.4	481.3	146.8	14.8	19.0
0.40	282.5	210.6	464.5	162.6	77.3	296.3	223.4	485.5	149.8	15.1	28.1
0.50	302.7	209.0	481.4	164.1	99.9	305.8	220.3	490.0	152.7	15.4	37.6
0.60	333.6	207.2	507.8	165.9	131.4	315.8	217.1	494.9	155.8	15.7	47.5
0.70	385.7	205.1	553.4	167.9	182.5	326.3	213.9	500.0	159.0	16.1	57.8
0.80	491.3	202.6	647.3	170.3	283.6	337.3	210.5	505.4	162.3	16.5	68.7

Similarly, due to increase in P_{HPG}, the specific enthalpy at state 11 (h_{11}) decreases slightly from 2697.7 kJ/kg at *D*=0.5 to 2696.4 at *D*=0.8. All these variations finally lead to an increase in $\dot{Q}_{HPG}$ in the double effect parallel system when *D* is increased. Similar variation was observed also in the reverse parallel system and this variation of increasing $\dot{Q}_{HPG}$ with *D* also holds well in the other cases of fixed component temperatures.

Further, $\dot{Q}_{LPG}$ decreases and $\dot{Q}_A$ and $\dot{Q}_C$ increases with *D* in both the parallel and reverse parallel systems at various test cases. At state 11, both the primary vapour flow rate and specific enthalpy ($\dot{m}_{11}$ and h_{11}) decreases slightly with *D* while the specific enthalpy at state 12 increases. Therefore, the LPG heat load ($\dot{Q}_{LPG}$) shows a decreasing trend in Table 4.11 at higher *D*. The mass flow rates of medium solution at LPG inlet ($\dot{m}_{10}$) and weak solution at LPG exit ($\dot{m}_{15}$) also increase with *D* in the parallel system. The specific enthalpy at state 10 (h_{10}) also increases with *D* mainly due to increase in temperature and reduction in solution concentration at state 10. The pressure, temperature, concentration and hence the enthalpy at state point 15 is not dependent of *D* variation. Accordingly, it affects the mass flow rates of the weak solution and secondary vapour stream leaving the LPG and these mass flow rates increase slightly with *D*. The enthalpy at state 14 is however independent of *D*. These changes in mass flow rates and enthalpies caused by *D* variation also affect the conditions downstream in the condenser and absorber. Condenser heat load ($\dot{Q}_C$) increases with *D* mainly due to increase in specific enthalpy value at state point 13. Mass flow rate and specific enthalpy at state 1 remains unchanged with *D*. Mass flow rate at state point 13 ($\dot{m}_{13}$) slightly reduces while the mass flow rate at state point 14 ($\dot{m}_{14}$) shows a marginal increase with *D*, hence these are not responsible for increase in $\dot{Q}_C$. Similarly, the mass flow rate and specific enthalpy of the refrigerant vapour at state 3 remain invariant with *D*. Since $\dot{m}_8$ and $\dot{m}_{15}$ both increase with *D,* therefore, the solution mass flow rate at state 17 ($\dot{m}_{15}$) also increases proportionately, causing an increase in the strong solution mass flow rate at absorber exit ($\dot{m}_4$). The specific enthalpies at state points 3 and 4 are however fixed and these don't vary with *D*. Only the enthalpy at state 17 shows some increase due to decrease in solution concentration and slight increase in the temperature at state 17.

Therefore, $\dot{Q}_A$ increases due to increase in mass flow rate at state 4 and mass flow rate and enthalpy at state points 4 and 17. Increase in $\dot{Q}_C$ and $\dot{Q}_A$ has a direct impact on the water circulation rate through these devices which is required for vapour condensation in the condenser and cooling of the absorber. In the reverse parallel system also, similar observations were made although the solution distribution is done in this system in a slightly different manner and some state points differ from that of the parallel configuration.

4.6.4 Performance comparison between double effect H_2O–LiCl and H_2O–LiBr systems

In Chapter 3, the comparison of performance between single effect H_2O–LiCl and H_2O–LiBr VARS at same operating conditions was presented and also similar comparison was available in the Refs. [17, 18]. However, in so far as double effect VARS is concerned, it was not done earlier. Here in this Chapter, the performance comparison between double effect H_2O–LiCl and H_2O–LiBr VARS configurations is provided under identical conditions of operating temperatures. The performance comparison between H_2O–LiCl and H_2O–LiBr operated double effect VARS configurations is shown in Table 4.12 at same operating conditions of $T_C = T_A$=33°C and T_E=8°C.

Results show that COP of all the double effect H_2O–LiCl VARS configurations are slightly higher than those of the H_2O–LiBr systems. In case of the series configuration, the COP difference, which is somewhat more at lower T_{LPG} and T_{HPG}, decreases however at higher T_{LPG} and T_{HPG}. The trend of decreasing COP difference at higher T_{LPG} and T_{HPG} is also the same in the parallel and reverse parallel configurations. The COP difference between the two systems is the highest in the reverse parallel configuration.

From Table 4.12, it is also seen that for the double effect series and parallel systems, the HPG pressures are slightly higher for the H_2O–LiCl solution pair compared to those for H_2O–LiBr at similar conditions of component temperatures. An increase in HPG pressure apparently implies higher pumping power for the solution pump at the absorber exit which however was not the case because the SP powers in case of the

H_2O–LiCl operated series, parallel and reverse parallel systems were drastically less compared to the H_2O–LiBr based systems. This was mainly due to lower mass flow rate of the strong solution at absorber exit ($\dot{m}_{ss}$) in respect of H_2O–LiCl solution. In fact, for a given cooling load (hence for the same refrigerant mass flow rate), the mass flow rates of weak and medium solutions are significantly less when the systems are operated with H_2O–LiCl solution pair. For the reverse parallel system, however, the HPG pressures are found to be slightly lower for H_2O–LiCl compared to H_2O–LiBr.

For the series configurations, the COP comparison is not shown for T_{LPG} above 71°C because this is the limit for the H_2O–LiCl series configuration at Case 1. In the parallel and reverse parallel configurations also, the COP comparison is not shown for T_{LPG} values above their corresponding limiting values. Of course, such limitation is not so restrictive in the H_2O–LiBr system. Double effect H_2O–LiBr systems can be operated over a wider range of T_{LPG} and it usually performs better at higher T_{LPG}. For example, a COP of 1.437 can be obtained by operating the H_2O–LiBr series configuration at T_{LPG} =80°C and T_{HPG} =120°C while maintaining the other component temperatures as indicated in Case 1 ($T_C = T_A$=33°C and T_E=8°C). For the H_2O–LiCl series configuration, the maximum possible COP is 1.428 and this occurs at T_{LPG}=71°C and T_{HPG}=105°C if it is operated with other components' temperatures as indicated in Case 1. Moreover, it would not be possible to operate the double effect H_2O–LiCl VARS configurations at T_{LPG}=80°C and T_{HPG}=120°C keeping other component temperatures fixed at $T_C = T_A$ =33°C and T_E=8°C due to the crystallization problem (solution concentration will exceed 50%). In order to operate the double effect H_2O–LiCl systems particularly at higher T_{LPG}, the condenser and absorber temperatures also need to be increased simultaneously. However, in that case, it would not be possible to obtain better COP at higher condenser and absorber temperatures.

4.7 Summary

The thermodynamic performance of double effect H_2O–LiCl VARS configurations (series, parallel and reverse parallel) was simulated in this study. Effect of components' temperature and distribution ratio (in case of parallel and reverse parallel system) on performance (COP), solution concentrations and components' heat loads was

investigated through parametric variation. Further, a performance comparison between double effect H_2O–LiCl and H_2O–LiBr VARS configurations was done. The following conclusions are made from the results obtained and the analysis performed.

- COPs of all the three double effect H_2O–LiCl VARS configurations are more at lower condenser and absorber temperatures and higher evaporator temperature.
- Usually with LPG temperature (T_{LPG}), the COP increases; however, depending on set temperatures in the other components (absorber, condenser and evaporator), T_{LPG} can't be increased beyond certain limit due to the limitation posed by maximum concentration exceeding 50% limit.
- At fixed temperatures in the other components, the maximum solution concentration is mainly controlled by T_{LPG} in the series configuration. However, in the parallel and reverse parallel configurations, both T_{LPG} and distribution ratio *'D'* controls the maximum solution concentration.
- Depending on set temperatures in the other components, the COPs of the double effect H_2O–LiCl VARS configurations are maximized at a particular combination of T_{LPG} and T_{HPG} . Moreover, the optimum COP of a given double effect H_2O–LiCl VARS is governed by an optimal temperature difference between T_{HPG} and T_{LPG} .
- Among the double effect H_2O–LiCl VARS configurations, the parallel configuration gives better COP compared to the series and reverse parallel configurations usually at higher T_{LPG} and T_{HPG} . At certain lower range of T_{LPG} and T_{HPG} however, the series flow configuration performs better than the parallel system.
- The distribution parameter *'D'* plays an important role in determining performance of the double effect parallel and reverse parallel flow configurations. Usually better system performance is obtained at lower *'D'* values, but the lower *D* limit is fixed by 50% maximum solution concentration limit in the double effect H_2O–LiCl parallel and reverse parallel systems. Further, at certain lower range of *D* values, the parallel

system shows better performance compared to the reverse parallel system while at higher *D* range, the reverse parallel system performs better than the parallel system. The extent to which the *D* value can be lowered in parallel and reverse parallel systems depends upon the components' temperatures.

- The performance comparison between the double effect H_2O–LiCl and H_2O–LiBr VARS configurations at same operating conditions showed better performance in respect of H_2O–LiCl systems. This is however the case at lower T_{LPG} and T_{HPG} only. This implies that it is possible to obtain better performance from the double effect H_2O-LiCl systems relatively at low T_{HPG} and T_{LPG}. The range of T_{LPG} is however limited in the H_2O–LiCl systems compared to the H_2O–LiBr systems where the system operation is possible for a wider range of T_{LPG}. At higher T_{LPG} and corresponding optimum T_{HPG}, certainly, the performance of the double effect H_2O–LiBr systems would be better than the corresponding double H_2O–LiCl systems.
- Further, the performance of double effect H_2O–LiCl parallel and series configurations were found superior to the reverse parallel configuration. Double effect H_2O–LiCl VARS configurations could certainly provide lot of opportunity in utilizing solar and other relatively low temperature waste heat sources.

Bibliography

[1] Won, S. H. and Lee, W. Y. Thermodynamic Design Data for Double-Effect Absorption Heat Pump Systems Using Water-Lithium Chloride Cooling. *Heat Recovery Systems and CHP,* 11: 41−48, 1991.

[2] Bellos, E., Tzivanidis, C., Pavlovic, S., and Stefanovic, V. Thermodynamic investigation of LiCl–H_2O working pair in a double effect absorption chiller driven by parabolic trough collectors. *Thermal Science and Engineering Progress,* 3:75–87, 2017.

[3] Patek, J. and Klomfar, J. Thermodynamic properties of the LiCl–H_2O system at vapour–liquid equilibrium from 273 K to 400 K. *International Journal of Refrigeration,* 31:287–303, 2008.

[4] Farshi, L. G., Mahmoudi, S. M. S., Rosen, M. A., and Yari, M. A. Comparative study of the performance characteristics of double-effect absorption refrigeration systems. *International Journal of Energy Research*, 36:182–192, 2012.

[5] Gomri, R. Second law comparison of single effect and double effect vapour absorption refrigeration systems. *Energy Conversion and Management,* 50: 1279–1287, 2009.

[6] Farshi, L. G., Mahmoudi, S. M. S., and Rosen, M. A. Analysis of crystallization risk in double effect absorption refrigeration systems. *Applied Thermal Engineering,* 31: 1712–1717, 2011.

[7] Talukdar, K. and Gogoi, T. K. Exergy analysis of a combined vapor power cycle and boiler flue gas driven double effect water–LiBr absorption refrigeration system. *Energy Conversion and Management,* 108: 468–477, 2016.

[8] Khaliq, A. and Kumar, R. Exergy analysis of double effect vapor absorption refrigeration system. *International Journal of Energy Research,* 32: 161–174, 2008.

[9] Gomri, R. and Hakimi, R. Second law analysis of double effect vapour absorption cooler system. *Energy Conversion and Management,* 49: 3343–3348, 2008.

[10] Wagner, W., Cooper, J. R., Dittmann, A., Kijima, J., Kretzschmar, H. J., Kruse, A., et al. The IAPWS Industrial Formulation 1997 for the thermodynamic properties of water and steam. *Journal of Engineering, Gas Turbine Power,* 122:150–81, 2000.

[11] Patek, J. and Klomfar, J. A computationally effective formulation of thermodynamic properties of LiBr–H_2O solutions from 273 to 500 K over full composition range. *International Journal of Refrigeration,* 29: 566–578, 2006.

[12] Kaita, Y. Thermodynamic properties of lithium bromide water solutions at high temperatures. *International Journal of Refrigeration,* 24: 374–390, 2001.

[13] Gebreslassie, B. H., Medrano, M., and Boer, D. Exergy analysis of multi-effect water–LiBr absorption systems: from half to triple effect. *Renewable Energy,* 35:1773–1782, 2010.

[14] Conde, M. R. Properties of aqueous solutions of Lithium and Calcium chlorides: formulations for use in air conditioning equipment design. *International Journal of Thermal Science,* 43:367–82, 2004.

[15] Patek, J. and Klomfar, J. Solid–liquid phase equilibrium in the systems of LiBr–H_2O and LiCl–H_2O. *Fluid Phase Equilibrium,* 250:138–49, 2006.

[16] Chaudhari, S. K. and Patil, K. R. Thermodynamic Properties of Aqueous Solutions of Lithium Chloride. *Physics and Chemistry of Liquids: An International journal,* 40:317–325, 2002.

[17] She. X., Yin, Y., Xu, M., and Zhang, X. A novel low-grade heat-driven absorption refrigeration system with LiCl–H_2O and LiBr–H_2O working pairs. *International Journal of Refrigeration,* 58: 219–34, 2015.